



Tectonic Deformation of the Western Qilian Shan in Response to the North–South Crustal Shortening and Sinistral Strike-Slip of the Altyn Tagh Fault Inferred From Geomorphologic Data

Zhidan Chen^{1,2}, Wenbin Xu^{1*}, Rui Liu³, An Li^{4*} and N. V. Koronovsky²

OPEN ACCESS

Edited by:

Wenjun Zheng,
Sun Yat-sen University, China

Reviewed by:

Daoyang Yuan,
Lanzhou University, China
Manoj Kumar Jaiswal,
Indian Institute of Science Education
and Research Kolkata, India
Bo Zhang,
China Earthquake Administration,
China

*Correspondence:

Wenbin Xu
wenbin.xu@csu.edu.cn
An Li
lian@ies.ac.cn

Specialty section:

This article was submitted to
Structural Geology and Tectonics,
a section of the journal
Frontiers in Earth Science

Received: 04 November 2021

Accepted: 18 January 2022

Published: 10 February 2022

Citation:

Chen Z, Xu W, Liu R, Li A and
Koronovsky NV (2022) Tectonic
Deformation of the Western Qilian
Shan in Response to the North–South
Crustal Shortening and Sinistral Strike-
Slip of the Altyn Tagh Fault Inferred
From Geomorphologic Data.
Front. Earth Sci. 10:808935.
doi: 10.3389/feart.2022.808935

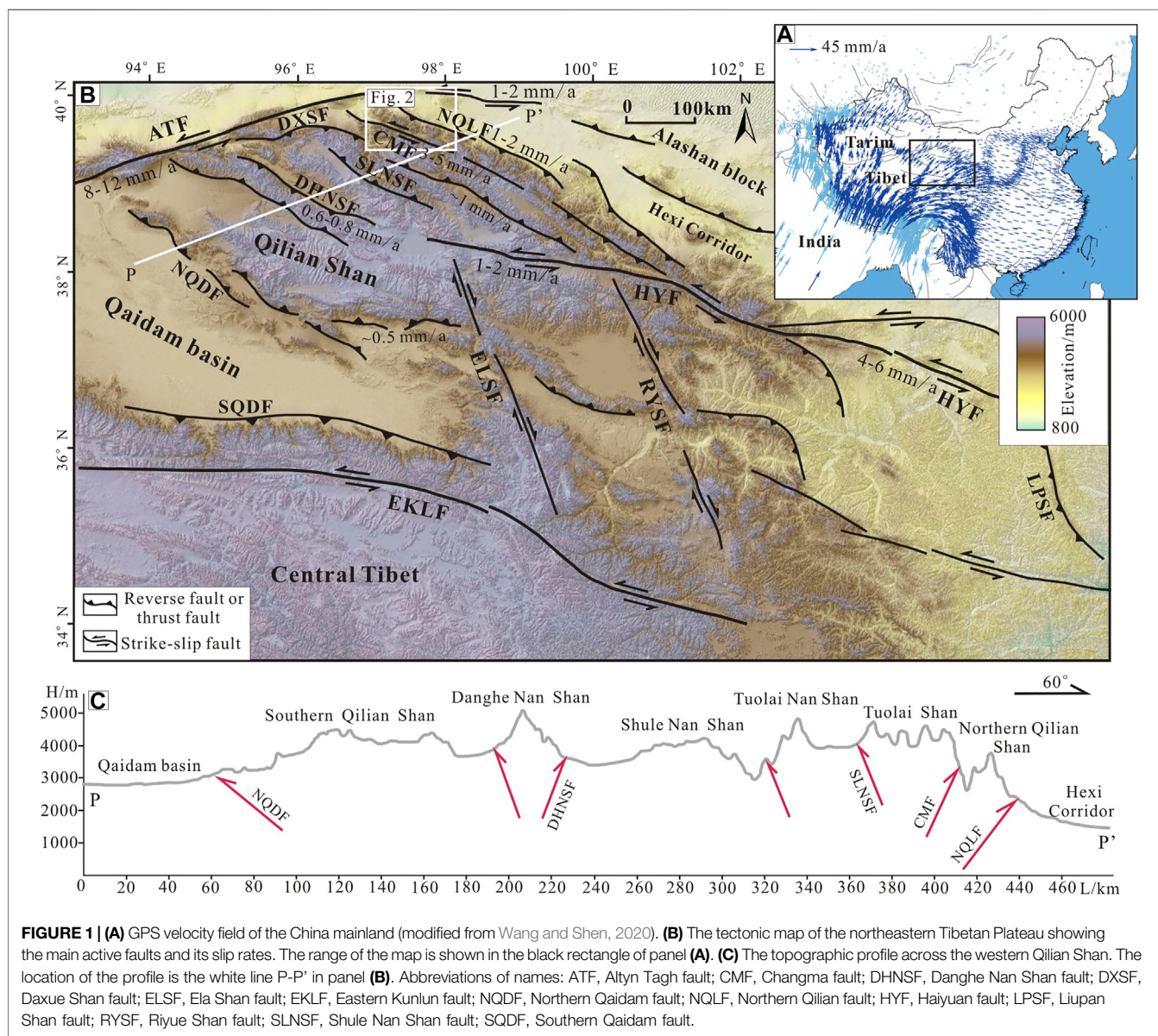
The tectonic deformation of a series of NWW-trending compressional band-shaped mountains and fault zones in the Qilian Shan, northeastern Tibet, plays an important role in absorbing the north–south crustal shortening of the Tibetan Plateau and accommodating the sinistral strike-slip of the Altyn Tagh fault. However, the deformation pattern of these mountains and fault zones in response to crustal shortening and sinistral strike-slip remains to be investigated. In this study, we present the slope map and swath profiles of the western Qilian Shan extracted from high-resolution digital elevation model (DEM) data and the fluvial geomorphologic characteristics of the Baiyang river in the northwestern Qilian Shan. Our data indicate that the crustal uplift of the northern Qilian Shan is stronger than that of the central and southern ranges of the Qilian Shan because of the high-terrain relief and stronger erosion. In addition, the deformed terraces of the Baiyang river documented the activity of NWW-trending faults in the western Qilian Shan. Based on the longitudinal profiles and ages of the deformed river terraces, the vertical slip rates of the Changma, Yumen, and Bainan faults in the western Qilian Shan since ~60 ka were constrained to be 0.31 ± 0.06 , 0.33 ± 0.02 , and 0.24 ± 0.02 mm/a, respectively. Based on the comparison with previous studies, we noticed that the rate of the vertical slip since the Late Quaternary of the northern Qilian fault of 1.5–2 mm/a is significantly higher than that of the Changma fault of 0.3–0.6 mm/a, which matches the terrain relief in the Qilian Shan and demonstrates that the northern Qilian Shan has been rising faster than its southern ranges. From the slip rates of the NWW-trending faults in the western Qilian Shan, we suggest that the crustal shortening is widely distributed in the NWW-trending compressional orogenic belts and fault zones across the Qilian Shan, among which the northern Qilian Shan and its frontal thrust system absorb the greatest shortening amount, whereas strike-slip faults within the Qilian Shan accommodate most of the sinistral strike-slip of the Altyn Tagh fault.

Keywords: western Qilian Shan, geomorphologic characteristics, river terrace, slip rate, crustal shortening, sinistral strike-slip

1 INTRODUCTION

The collision and post-collisional convergence between India and Eurasia have caused crustal shortening and thickening and led to the generation of the magnificent mountain ranges of the Himalayas and Tibetan Plateau (Molnar and Tapponnier, 1975; England and Houseman, 1986; Harrison et al., 1992; Yin and Harrison, 2000). Since the onset of the Indo-Asian collision at 65–50 Ma, the Himalayan-Tibetan orogen has absorbed at least 1,400 km of crustal shortening (Yin and Harrison, 2000; Ding et al., 2017), which have been transformed into the rapid uplift of mountains (e.g., Harrison et al., 1992; Wang et al., 2014), thrusting and strike-slip of faults (e.g., Molnar and Tapponnier, 1975; Zhang et al., 2004), lateral extrusion of blocks (e.g., Tapponnier and Molnar, 1976; Hodges et al., 2001), and shrinking and extinction of basins (e.g., Wang et al., 2014;

Ding et al., 2017). The northward expansion of the Tibetan Plateau led to the growth of a series of compressional orogenic belts in central Asia. Among them, the Qilian Shan (Shan means “mountains” in Chinese), an orogenic belt in the northeastern margin of the Tibetan Plateau, is a typical example (Wang et al., 2016). The Qilian Shan is located in the convergence zone of the Tibetan, Tarim, and Alshan blocks, that is, the transition region from the plateau ranges to basins in the north, and plays an important role in accommodating the tectonic deformation in the northern plateau (Zuza et al., 2016). Recent results based on the stratigraphy and apatite fission track chronology suggest that the Qilian Shan began to uplift during the Late Miocene (14–10 Ma) (Wang et al., 2016; Zheng et al., 2017), much later than the Indo-Asian collision (Wang et al., 2014; Ding et al., 2017). Although the Qilian Shan with an average altitude of >4,000 m was formed relatively later, its area exceeds 2,000 km². Its enormous size



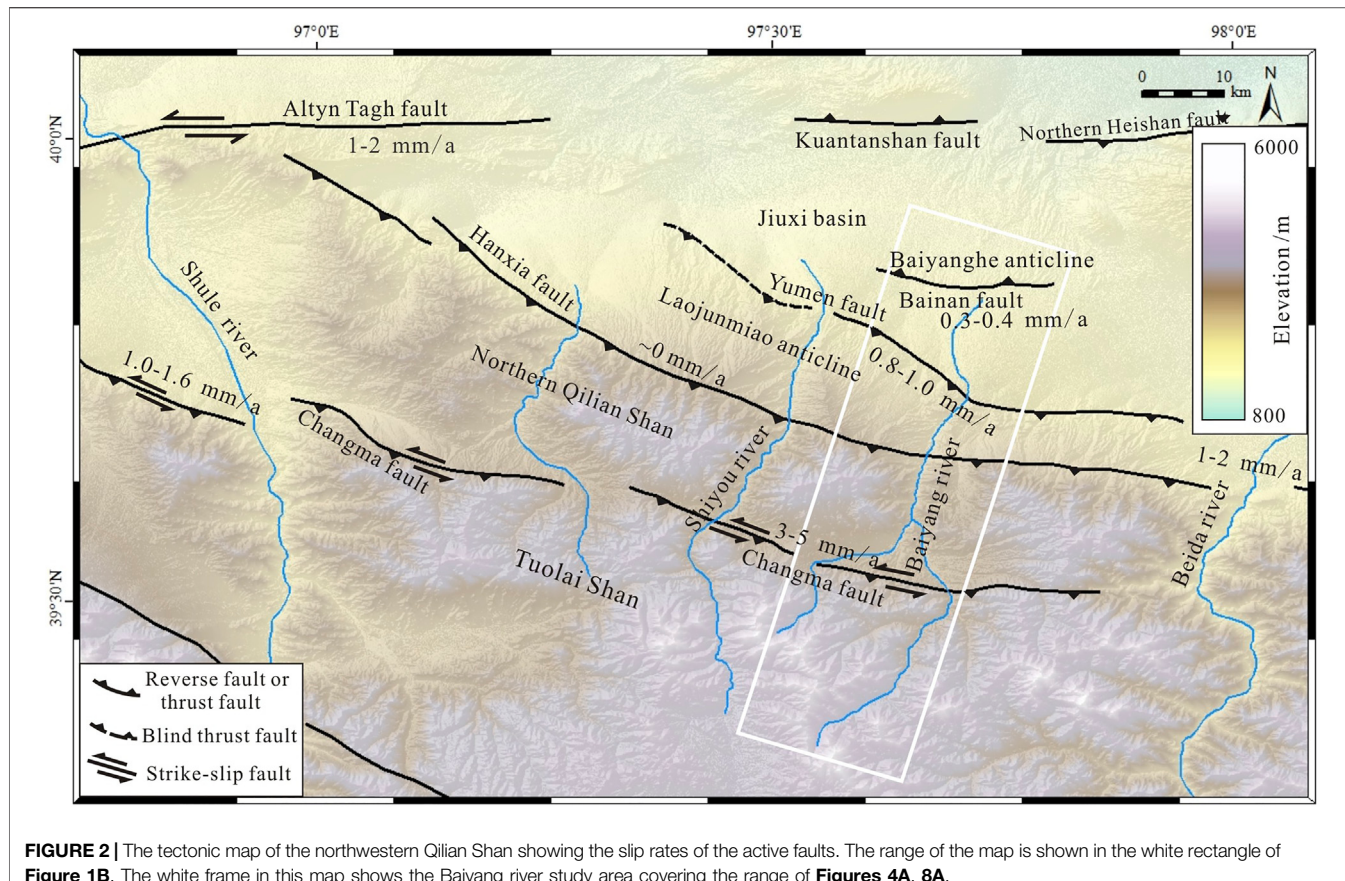


FIGURE 2 | The tectonic map of the northwestern Qilian Shan showing the slip rates of the active faults. The range of the map is shown in the white rectangle of **Figure 1B**. The white frame in this map shows the Baiyang river study area covering the range of **Figures 4A, 8A**.

makes it a non-negligible part of studies of the tectonic deformation of the plateau (**Figure 1B**).

The Qilian Shan absorbs the north–northeast (NNE) crustal shortening of the Tibetan Plateau and accommodates the sinistral strike-slip of the Altyn Tagh fault. Based on the Global Positioning System (GPS) velocity field, the present-day shortening rate between India and Eurasia is 40–50 mm/a (millimeters per year) of which 15–20 and 20–30 mm/a are absorbed by the Himalayan tectonic belt and the deformation within the Tibetan Plateau and surrounding mountains, respectively (**Figure 1A**) (Zhang et al., 2004; Wang and Shen, 2020). The crustal shortening rate across the Qilian Shan is 5.5 ± 1.5 mm/a, accounting for 15%–17% of the total convergence rate between India and Eurasia, which is mainly absorbed by the uplift of mountains and deformation of five large-scale folded fault belts (Zhang et al., 2004). The Altyn Tagh fault on the west side of the Qilian Shan is a continental sinistral strike-slip fault in the northern plateau. The GPS measurements revealed that the sinistral slip rate of the Altyn Tagh fault decreases from 8 to 12 mm/a in the middle section to 1–2 mm/a in the easternmost section after crossing the Qilian Shan (**Figure 1B**) (Zhang et al., 2004; Liu J. et al., 2020; Wang and Shen, 2020), indicating that the Qilian Shan accommodates ~8 mm/a of the sinistral strike-slip of the Altyn Tagh fault. However, the focus of previous studies was mainly placed on the tectonic deformation of boundary fault belts in the Qilian Shan, especially the northern Qilian Shan and its

frontal thrust (e.g., Hetzel et al., 2002; Hetzel et al., 2004; Zheng et al., 2013a; Hu et al., 2015; Liu R. et al., 2017; Liu X.-W. et al., 2017; Yang et al., 2018a; Yang et al., 2018b; Liu X.-w. et al., 2019; Liu X. et al., 2019; Hetzel et al., 2019; Yang et al., 2020; Hu et al., 2021; Li et al., 2021). The knowledge of the sinistral strike-slip and the compressional deformation within the Qilian Shan is insufficient, which restricts the overall understanding of the tectonic deformation in the northern plateau.

Spatial analysis and geomorphological quantitative studies are powerful tools for studying tectonic deformation within the Qilian Shan. Based on high-resolution digital elevation model (DEM) data and geomorphic parameters, such as the slope and relief extracted in this study, the spatial variation of the terrain relief can be determined. A series of north–south rivers flow perpendicularly through the band-shaped mountains and fault zones in the western Qilian Shan and have inevitably been affected by tectonic activity (**Figure 2**). The geomorphologic characteristics of these rivers reflect the tectonic deformation of the mountain ranges and tectonic belts (Chen and Koronovskii, 2020). It has been proven that the slip rates of the faults and fold belts can be constrained by studying deformed landforms along the active Qilian Shan front and in its foreland (e.g., Hetzel et al., 2002; Hetzel et al., 2004; Hu et al., 2015; Liu X.-W. et al., 2017; Yang et al., 2018a; Yang et al., 2018b; Liu X.-w. et al., 2019; Liu X. et al., 2019; Hetzel et al., 2019; Chen and Koronovskii, 2020; Liu R. et al., 2020). In this study, field surveys

and topographic measurement were applied to analyze the fluvial geomorphologic characteristics of the western Qilian Shan. By measuring the displacements and ages of deformed river terraces, we obtained the long-term slip rates of the main faults in the study area. All above-mentioned results were used to explain the tectonic deformation, strain distribution, and deformation pattern in the western Qilian Shan.

2 TECTONIC SETTING OF THE STUDY AREA

The Qilian Shan is the northeastern leading edge of the Tibetan Plateau, resulting from the northward expansion of the plateau. The overall tectonic trend of the Qilian Shan is approximately N65°W, almost perpendicular to the direction of the relative movement between the Indian and Eurasian plates (Zhang et al., 2004). A series of band-shaped mountains, compressional basins, and fault and fold zones in the Qilian Shan are distributed in the NWW direction, demonstrating that the tectonic deformation of the Qilian Shan is characterized by compression (**Figure 1B**). Based on GPS data, the crustal shortening rate between the Qaidam Basin and Alshan Block is 5.5 ± 1.5 mm/a, which is largely absorbed by the NWW-trending mountains and fault zones in the Qilian Shan (Zhang et al., 2004).

Our study area is the western Qilian Shan, which is bounded by the Altyn Tagh fault to the west and the Haiyuan fault to the east. From south to north, five large-scale NWW-trending compressional fault zones can be observed, that are the northern Qaidam, Danghe Nan Shan, Shule Nan Shan, Changma, and northern Qilian faults (**Figures 1B,C**). The results of previous studies showed that the tectonic deformation of the NWW-trending mountains and fault zones in the western Qilian Shan plays a significant role in absorbing the NNE crustal shortening of the plateau and accommodating a large amount of sinistral strike-slip components of the Altyn Tagh and Haiyuan faults (Zhang et al., 2007; Zheng et al., 2009; Zheng et al., 2013b; Liu J. et al., 2020). These mountains and fault zones obliquely intersect the Altyn Tagh and Haiyuan faults at low angles (**Figure 1B**). Based on GPS data, the sinistral strike-slip rate in the middle section of the Altyn Tagh fault is 8–12 mm/a and decreases to 1–2 mm/a in the eastern section (**Figure 1B**) (Zhang et al., 2007; Zheng et al., 2009; Zheng et al., 2013b; Liu J. et al., 2020). The geological results suggest that the sinistral strike-slip rate of the Altyn Tagh fault in the Holocene was 17.5 ± 2.2 mm/a in the midwest, 11 ± 3.5 mm/a in the middle, and 2.2 ± 0.2 mm/a in the east (Xu et al., 2005). The sinistral strike-slip rate of the Altyn Tagh fault decreased from west to east and considerable sinistral strike-slip was absorbed by the tectonic deformation in the western Qilian Shan. Contrary to the decreasing trend of the Altyn Tagh fault, the slip rate of the Haiyuan fault gradually increased from west to east. Based on GPS data, the sinistral strike-slip rate of the Haiyuan fault is only 1–2 mm/a in the west adjacent to Danghe Nan Shan and 4–5 mm/a in the middle section near the Tuolai Nan Shan, but it reaches 4–6 mm/a at the northern margin of the Qilian Shan (**Figure 1B**) (Zheng et al., 2009; Zheng et al., 2013b), which

suggests that ~4 mm/a of the sinistral strike-slip in the western Qilian Shan has been transferred into the Haiyuan fault. The variation in the slip rates of the Altyn Tagh and Haiyuan faults indicates that the western Qilian Shan is an important transition zone for the accommodation of the sinistral strike-slip of these two large-scale faults, where a large proportion of sinistral strike-slip components of the Altyn Tagh fault has been absorbed and partially transferred into the Haiyuan fault by the NWW-trending mountain building and faulting within the western Qilian Shan.

The northwestern Qilian Shan represents the junction zone of the Qilian, Tarim, and Alashan blocks where tectonic deformation is characterized by crustal shortening and surface uplift (Chen and Koronovskii, 2020). A series of north–south rivers flow through the NWW-trending band-shaped mountains and active fault zones in the western Qilian Shan. These rivers provide typical geomorphologic markers for studying the tectonic deformation in this area. In this study, the Baiyang river, one of the largest north–south rivers in the northwestern Qilian Shan, was selected as the research object (**Figure 2**). Four NWW-trending fold-and-thrust zones are developed from south to north in the Baiyang river catchment, that is, the Changma, Hanxia, and Yumen faults and its anticline (Laojunmiao anticline) and the Bainan fault and its anticline (Baiyanghe anticline) (**Figure 2**) (Liu R. et al., 2017; Chen and Koronovskii, 2020). These faults are subject to compressional deformation in the NNE direction and the sinistral strike-slip of the Altyn Tagh fault. Their trend is consistent with the principal stress field of the Qilian Shan. Based on topographic surveys and ^{14}C dating, Zheng et al. (2013a) determined the left-lateral and thrust slip rates of 1.17 ± 0.07 and 0.25 mm/a of the Changma fault. However, Luo et al. (2013) constrained the left-lateral and thrust slip rates of the Changma fault to be 1–3 mm/a and 0.3–0.6 mm/a; Du et al. (2020) estimated the left-lateral slip rates of the Changma fault to be 3–5 mm/a. Previous studies on the constraint of slip rates of the Changma fault differ greatly. Using similar methods, Liu X.-w. et al. (2019) derived a vertical slip rate of 0.9 ± 0.1 mm/a and a shortening rate of 1.9 ± 0.5 mm/a for the Yumen blind thrust in the Qilian Shan foreland and Hetzel et al. (2002, 2019) obtained a vertical slip rate of 0.35 ± 0.05 mm/a for the Bainan fault and a horizontal shortening rate of 2.0 ± 0.3 mm/a for the northern Qilian Shan frontal thrust. Most of studies show that the shortening rates of the northern Qilian Shan fault system vary in the range of 1–2 mm/a (e.g., Hetzel et al., 2004; Zheng et al., 2013a; Hu et al., 2015; Liu X.-W. et al., 2017; Yang et al., 2018a; Yang et al., 2018b; Liu X.-w. et al., 2019; Liu X. et al., 2019; Hetzel et al., 2019).

3 MATERIALS AND METHODS

3.1 Geomorphologic Spatial Analysis Based on the Digital Elevation Model

Geomorphologic parameters, such as the slope and slope direction, extracted from high-resolution DEM data can provide qualitative and quantitative constraints for studying the tectonic deformation in orogenic belts (e.g., Chu, 2015). In

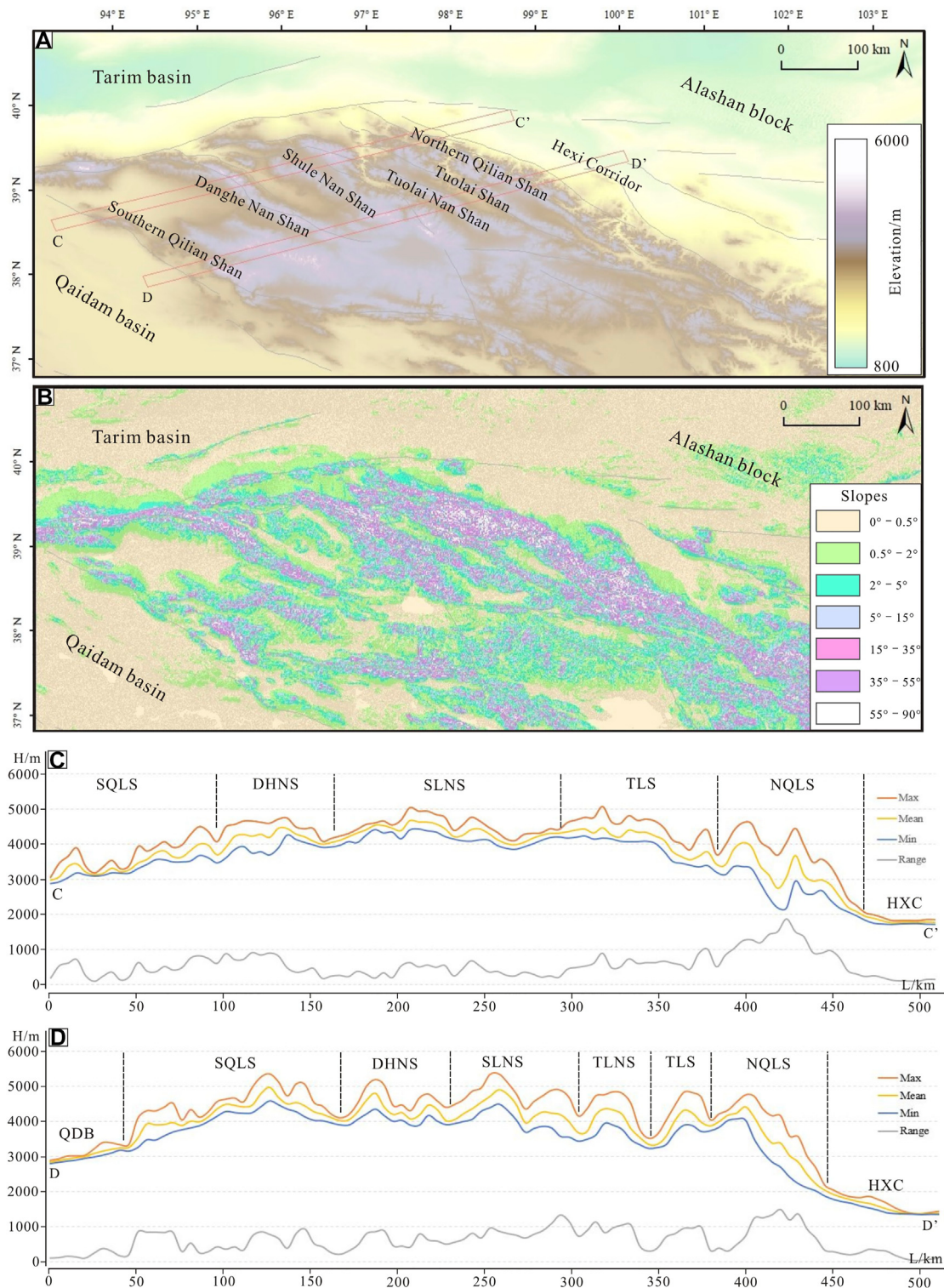


FIGURE 3 | (A) The DEM image of the Qilian Shan. **(B)** The slope map of the Qilian Shan. The gray lines represent active faults in the Qilian Shan. **(C,D)** are swath profiles on the western Qilian Shan. The locations of the swath profiles are shown in the red rectangles of panel **(A)**. The Max, Mean, Min, and Range curves represent the maximum, average, minimum, and standard deviation (difference between the maximum and minimum) of elevations in the swath ranges, respectively. Abbreviations of names: SQLS, Southern Qilian Shan; DHNS, Danghe Nan Shan; SLNS, Shule Nan Shan; TLNS, Tuolai Nan Shan; TLS, Tuolai Shan; NQLS, Northern Qilian Shan; QDB, Qaidam basin; HXC, Hexi Corridor.

this study, we obtained slope parameters based on DEM data with a precision of 30 m and developed the slope map of the Qilian Shan using ArcGIS software (**Figure 3B**), which accurately reflects the spatial variation of the terrain slope in the Qilian Shan. Before analyzing the spatial variation of the terrain slope, a reasonable slope classification system must be established. In this study, based on the slope classification developed by the Geomorphology Survey and Mapping Committee of the International Geographical Union, we classified the slope grades as follows: 0° – 0.5° , 0.5° – 2° , 2° – 5° , 5° – 15° , 15° – 35° , 35° – 55° , and 55° – 90° , representing the plain, gentle slope, moderate slope, steep slope, very steep slope, cliff, and vertical wall, respectively (**Figure 3B**) (Chu, 2015; Cheng et al., 2019). In the slope map, different slopes were expressed using different colors to present the spatial variation of the slopes.

Topographic swath profiles have an advantage over conventional topographic linear profiles with respect to the evaluation of the effects of vertical surface movements in the investigation of fluvially sculpted topography. Based on topographic swath profiles derived from DEM data, a simple linear profile can be expanded into a rectangular swath profile and the elevation in a given swath area can be calculated as statistical parameters (maximum, mean, minimum, and standard deviation), which reflect the terrain relief in the study area and compensate for the deficiencies of single linear topographic profiles (Chu, 2015). In this study, we used the 3D analyst tools of ArcGIS to extract two swath profiles across the western Qilian Shan, perpendicular to the strike of the mountains and faults. Each profile has a width of 5 km and length exceeding 500 km (**Figure 3A**). Then, we divided each profile into 100 units, each of which is a square of $5 \times 5 \text{ km}^2$. Based on the elevation from DEM, we derived the maximum (Max), average (Mean), minimum (Min), and Range values (the difference between Max and Min) of elevation for each unit and plotted four curves in the swath ranges, respectively. (**Figures 3C,D**).

3.2 Topographic Surveys of the Fluvial Geomorphology

The fluvially sculpted topography on the Earth's surface is the result of interactions among the tectonics, erosion, and climate (Lavé and Avouac, 2001). To analyze the coupling between the fluvial topography and tectonic movements, it is crucial to accurately identify geomorphic markers that can reflect tectonic deformation. The results of previous studies suggested that climate change is the driving force of deep incision and the formation of terraces of rivers in the northern Qilian Shan because the regional fluvial incision rates are significantly higher than the vertical slip rates of the northern Qilian thrust (e.g., Hetzel et al., 2006; Yang et al., 2020). Despite the inconsistencies of the incision and vertical slip rates, numerous fluvial geomorphic markers can be used to reflect the tectonic deformation in orogenic belts such as hanging valleys, bedrock gorges, steep V-shaped channels, fluvial strath terraces, etc. (Chen and Koronovskii, 2020). Through a field investigation, we comprehensively analyzed the geomorphic

features of the reaches of the Baiyang river catchment, including the valley contour, riverbed characteristics, heights of the valleys, types, and composition of terraces, etc. Based on the distribution of mountain ranges and faults and fluvial geomorphologic features, the Baiyang river can be divided into upper, middle, and lower reaches. The sections south of the Changma fault, from the Changma fault to the Yumen fault, and north of the Yumen fault were classified as the upper, middle, and lower reaches, respectively (**Figure 4A**).

3.3 Measurement of the Displacement and Ages of Deformed Terraces

River terraces have been deformed due to the continuous activity along faults in the northern Qilian Shan. In turn, the displacement of the river terraces reflects the movement of these faults. By measuring the displacement of the terraces and determining their ages, the rates of the long-term slip of these faults since the Late Quaternary can be obtained (e.g., Liu R. et al., 2017; Yang et al., 2018a; Yang et al., 2018b; Liu X.-w. et al., 2019; Liu X. et al., 2019; Chen and Koronovskii, 2020). The key to deriving the long-term slip rates of faults is to accurately measure the offsets and ages of terraces. In this study, the differential GPS with a centimeter accuracy was used to obtain the elevation of terraces above the riverbed near faults, based on which the longitudinal profiles of the river terraces were established. We first investigated the development of river terraces near the faults and divided the river terraces into different levels based on the elevation, distribution areas, and composition. Along the Changma fault, we identified three terrace levels and named them T1 to T3 (**Figures 5A,B**). Along the Hanxia and Yumen faults, we divided the terraces into 5–6 levels (**Figures 6A,B,D**). Along the Bainan fault and its anticline, we identified five terrace levels (**Figures 7B,C**). Then, we used the Trimble R10 GNSS measurement system to obtain the elevation of terraces. In this way, we obtained the elevation data of T1–T3 terraces near the Changma fault, T1–T5 near the Yumen fault, T1–T5 near the Bainan fault and the riverbed (T0). At last, the longitudinal profiles of the terraces were established to derive the offsets of the terraces due to faulting. T3 along the Changma fault and T5 along the Yumen fault represent the regional terraces in the upper and middle reaches and its ages are also similar, demonstrating that these two terraces are comparable (**Table 1**).

We employed two dating methods (optically stimulated luminescence, OSL, and terrestrial cosmogenic nuclide dating, ^{10}Be) to estimate the ages of the offset terraces. Near the Changma fault, we collected the OSL dating sample from the loess layer approximately 2 m below the surface of T3 (**Figure 5A**). Between the Hanxia fault and Yumen fault, we collected the ^{10}Be dating samples of T3 and T5 from the terrace well-developed section (**Figure 6A**). On the north side of the Bainan fault, we collected ^{10}Be samples from all terraces (**Figure 7B**). All sampled terraces are well-developed regional terraces in their respective sections. The dating procedures can be referred to our previous study of Liu R. et al. (2020). Some results of offsets and ages of fault terraces have been published in our previous works (Liu R. et al.,

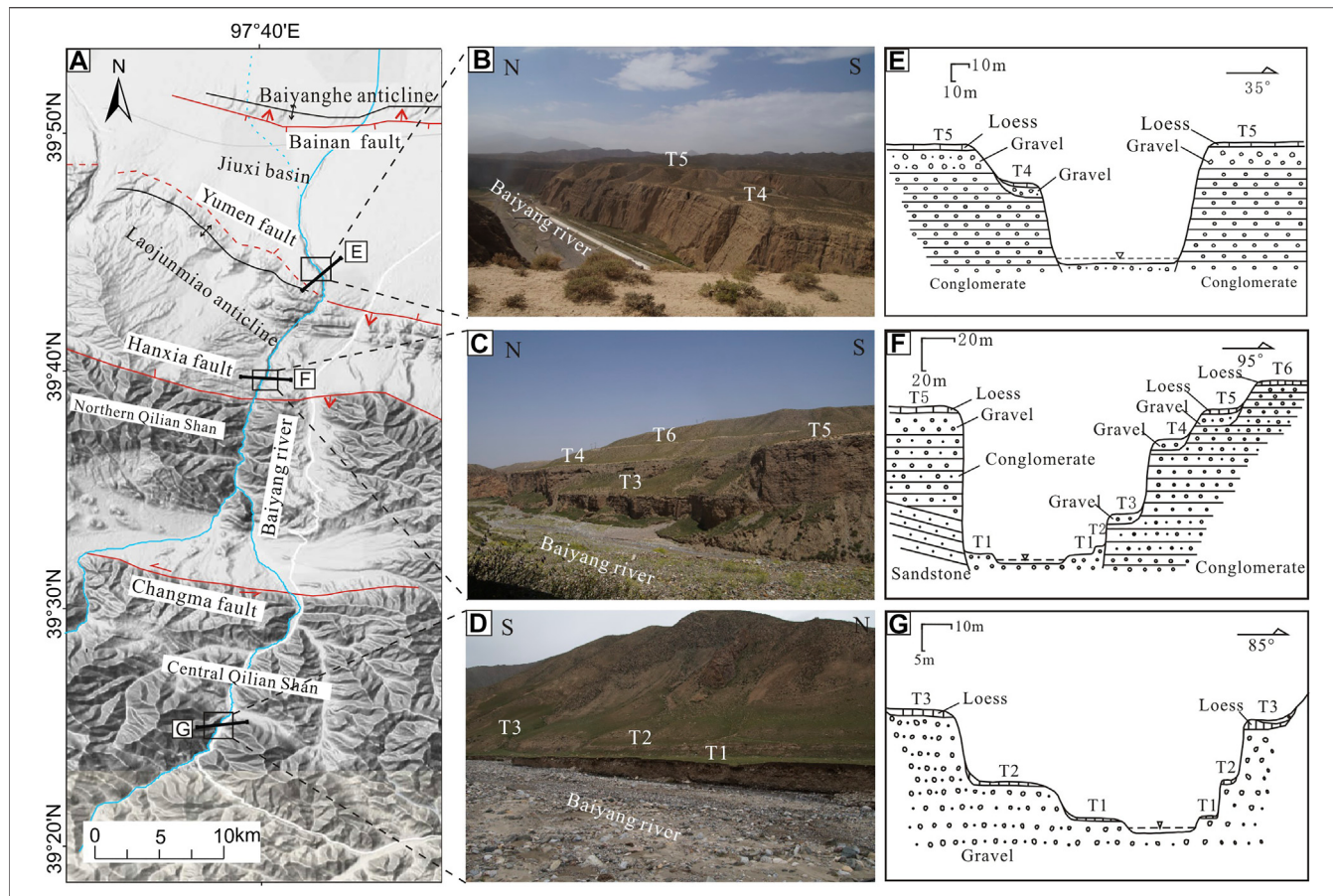


FIGURE 4 | (A) The topographic map of the Baiyang river catchment. The range of the map is shown in the white frame of **Figure 2**. **(B–D)** are the regional terrace photographs of the lower, middle and upper reaches of the Baiyang river. Black rectangles of panel **(A)** show the locations of these photographs. **(E–G)** are the representative geologic transects of river terraces of the lower, middle and upper reaches, showing the terrace levels and the composition of terraces. The thick black lines in panel **(A)** denote the positions of these transects (modified from Chen and Koronovskii, 2020).

2017; Chen and Koronovskii, 2020). In this study, we reorganized these data for our research purpose and listed them in **Table 1**.

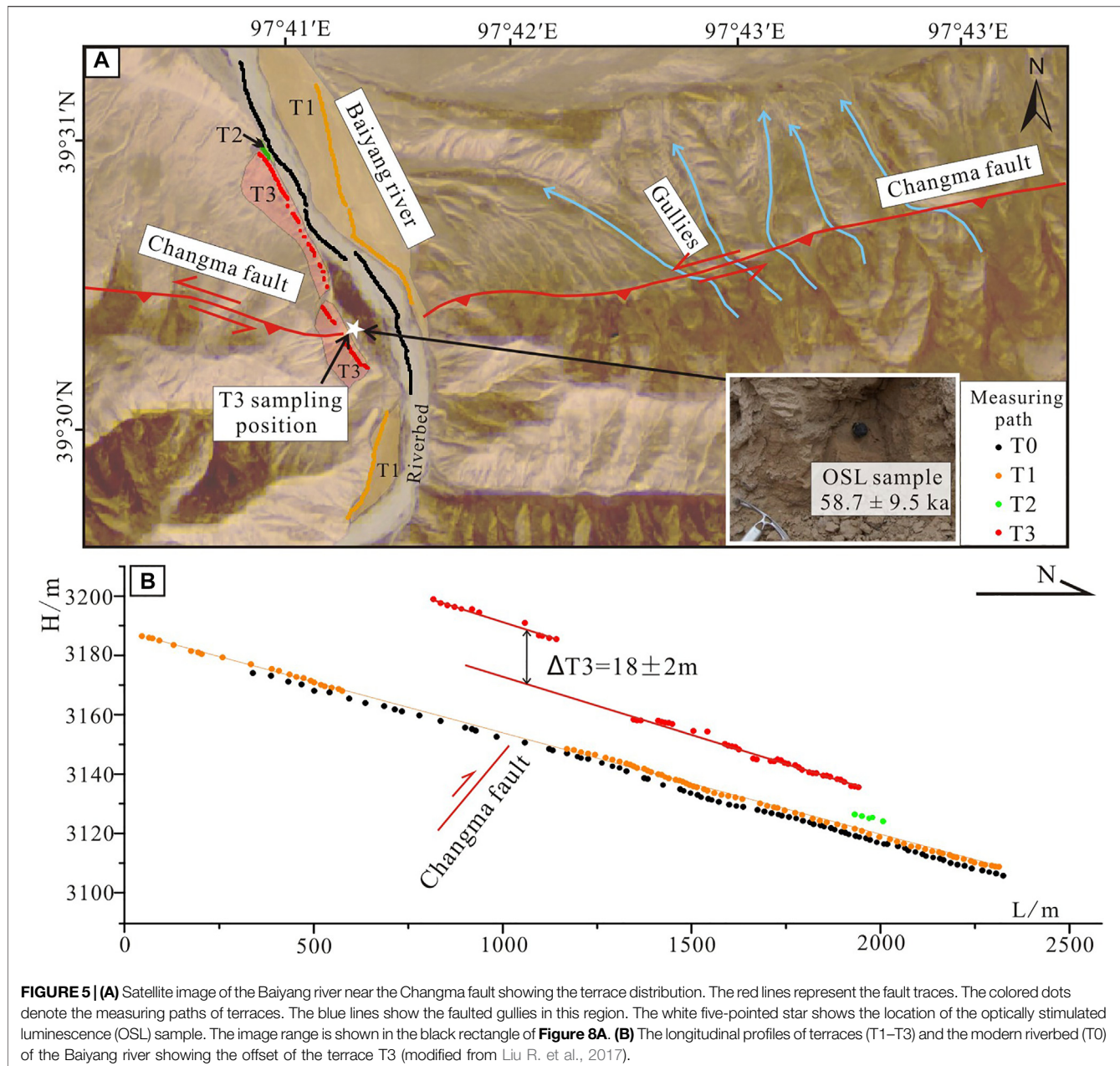
4 RESULTS

4.1 Slope Map and Swath Profiles Based on the Digital Elevation Model

To characterize the topographic features of the Qilian Shan, a slope map and two swath profiles based on high-resolution DEM data of the Qilian Shan were extracted in this study (**Figures 3A–D**). The slope map shows that plains, gentle slopes, and moderate slopes are mainly distributed in the basins and valleys within and around the Qilian Shan and are widely distributed in the south of the Qilian Shan. However, they are limitedly distributed in band-shaped intermontane basins in the central and northern Qilian Shan (**Figure 3B**). Areas with steep slopes are strictly limited to the foothills of mountain ranges. Cliffs and vertical walls best represent the high-relief topography and are widespread in all NWW-trending band-shaped mountains of the Qilian Shan, but their distributions differ. In the northern Qilian

Shan, they are widely distributed, extending from the northern margin of the Qilian Shan to the Tuolai Nan Shan, accounting for more than 60% of the entire distribution of cliffs and vertical walls (**Figure 3B**). In the central Qilian Shan, they are in the top areas of the Shule Nan Shan and the Danghe Nan Shan, accounting for ~30% of the distribution of cliffs and vertical walls. However, in the southern Qilian Shan, cliffs and vertical walls are rare; they are distributed at the peaks of mountain ranges, accounting for less than 10% of the distribution of cliffs and vertical walls (**Figure 3B**). Therefore, the spatial variation of the slopes shows that the distribution of areas with high slopes in the northern Qilian Shan is significantly larger than that in the southern and central Qilian Shan.

We extracted two swath profiles with an extension direction perpendicular to the strike of the mountains and plotted four curves (Max, Mean, Min, and Range curves) based on calculating the elevations in the swath ranges (**Figures 3B–D**). The range curve best represents the terrain relief in the study area. In the western profile (**Figure 3C**, swath profile C-C'), the range is comparatively low in the southern and central areas, reaching ~800 m in the southern Qilian Shan, ~1,000 m in the Danghe Nan



Shan, and the minimum of 700 m in the Shule Nan Shan. From the Tuolai Nan Shan to the northern Qilian Shan, the range significantly increases. In the Tuolai Nan Shan, the range steadily varies between 700 and 1,000 m, but that is above 1,000 m within a width of 70 km in the northern Qilian Shan and rapidly reaches the maximum of 2,000 m in the middle of the northern Qilian Shan (**Figure 3C**). In the eastern profile (**Figure 3D**, swath profile D-D'), the range is generally larger than that in the western profile, especially in the central Qilian Shan, and has a greater advantage of 200–300 m in the same mountain ranges. However, the range reaches maxima in the northern Qilian Shan in both profiles. In the eastern profile, the range reaches up to 1,000 m within a width of 35 km in the

northern Qilian Shan, with a maximum of 1,400 m (**Figure 3D**).

In summary, the topographic slope map and two swath profiles of the Qilian Shan show that the distribution of the high-relief terrain and the range value reach maxima in the northern Qilian Shan, demonstrating that the terrain relief in the northern Qilian Shan is much greater than that in the central and southern regions. The high terrain relief, in general, results from intense erosion, which is closely related to tectonics and climate. However, located in a same region, the mountains in the Qilian Shan have similar climatic conditions. Thus, the terrain relief in the northern Qilian Shan might be related to the rapid surface uplift in the northern Qilian Shan. Furthermore, the

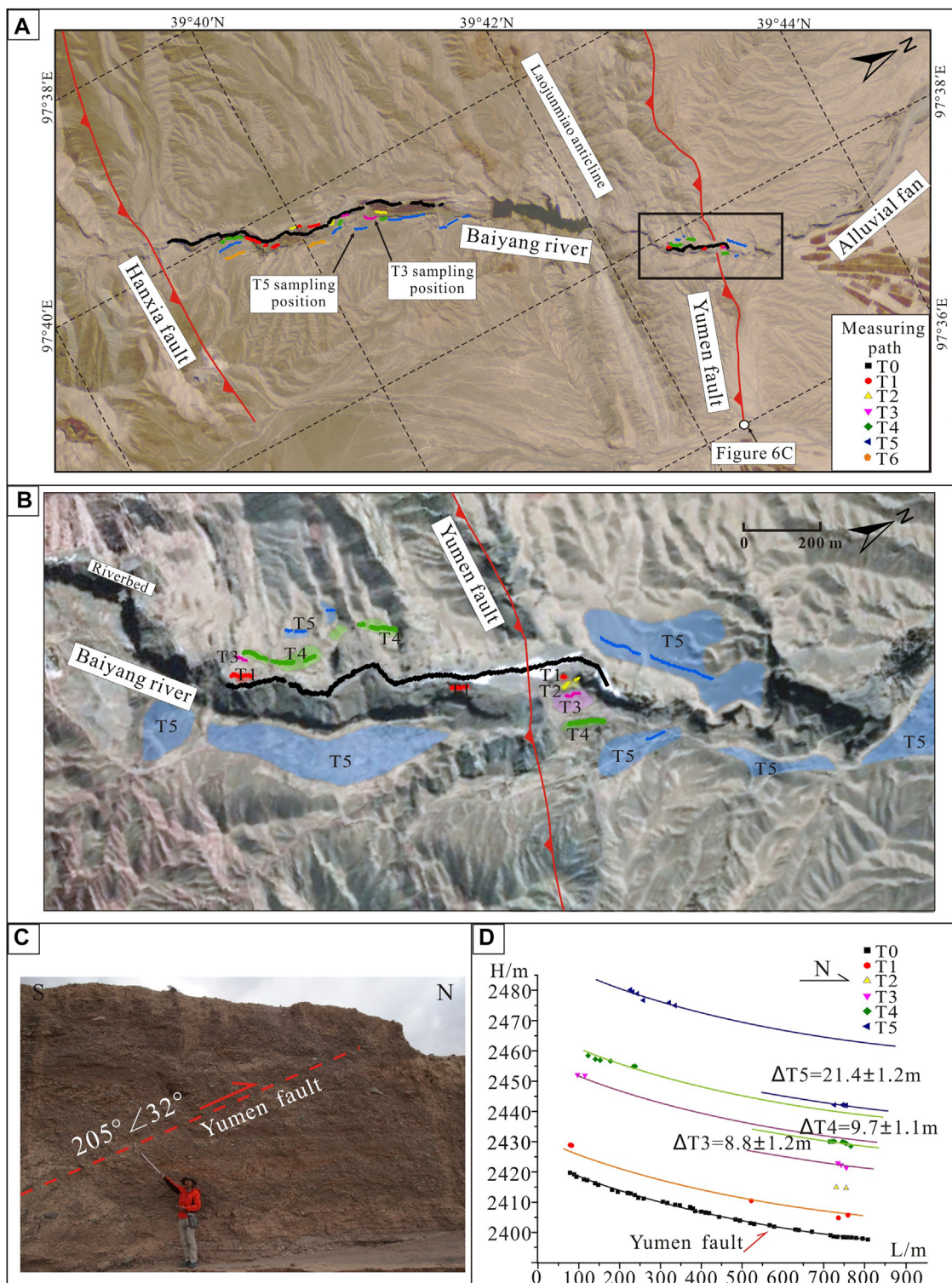


FIGURE 6 | (A) Satellite image of the Baiyang river in the northern Qilian Shan front. The red lines represent the fault traces. The colored dots denote the measuring paths of terraces. The ^{10}Be sampling positions of T3 and T5 terraces have been exhibited. The image range is shown in the black rectangle of **Figure 8A**. **(B)** Satellite image of the Baiyang river near the Yumen fault showing the terrace distribution. The image range is shown in the black rectangle of **(A)**. The colored dots denote the measuring paths of terraces (T1-T5). **(C)** The photograph of fault scarp of the Yumen fault in the alluvial fan. The location of photograph is shown in the **(A)**. **(D)** The longitudinal profiles of terraces (T1-T5) and the modern riverbed (T0) of the Baiyang river near the Yumen fault. The measuring paths have been shown in the **(B)** (Chen and Koronovskii, 2020; revised).

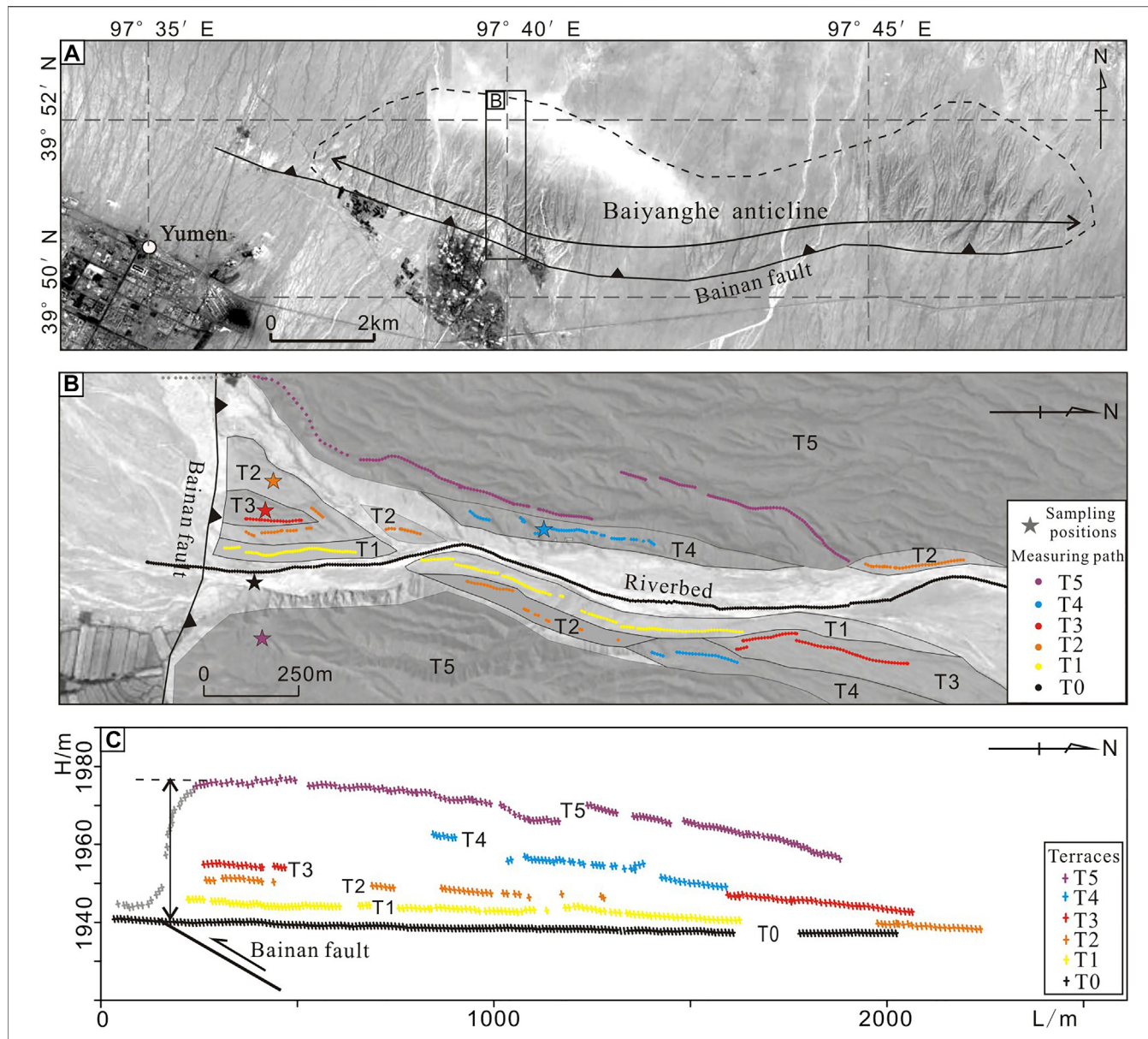


FIGURE 7 | (A) Satellite image of the Baiyang river near the Bainan fault. The image range is shown in the black rectangle of **Figure 8A**. **(B)** The distribution map of terraces along the Bainan fault. The colored dots denote the measuring paths of terraces. The colored five-pointed stars show the ^{10}Be sampling positions. The range of the measurement is shown in the black rectangle of panel **(A)**. **(C)** The longitudinal profiles of terraces (T1–T5) and the modern riverbed (T0) of the Baiyang river. The measuring paths are the yellow dots shown in the panel **(B)** (Liu et al., 2017a; revised).

research results of the Longmen Shan, the eastern margin of the Tibetan Plateau, also suggested that crustal deformation and topographic relief in mountain ranges are largely coupled (Hubbard and Shaw, 2009).

4.2 Geomorphologic Characteristics of the Baiyang River

The Baiyang river is a north-south river in the northern Qilian Shan. It originates within the Qilian Shan and flows northward through the northern mountain ranges of the Qilian Shan,

roughly perpendicular to the strike of the mountains and faults. After crossing the mountain ranges, it continues to incise piedmont alluvial fans and flows into the Jiuxi Basin (**Figure 4A**). The Baiyang river flows through four active faults, which from south to north are the Changma, Hanxia, Yumen, and Bainan faults (**Figure 4A**). In this study, the Baiyang river was divided into upper, middle, and lower reaches based on the distribution of faults and fluvial topographic characteristics (Liu R. et al., 2017; Chen and Koronovskii, 2020).

In the upper reaches of the Baiyang river, wide and U-shaped valleys are developed. The riverbeds are wide (up to 50–150 m

TABLE 1 |The displacements and ages of terraces and slip rates of faults in the Baiyang river.

Faults	Terraces	Offsets (m) ^a	Ages (ka) ^a	Vertical slip rate (mm/a)
Changma	T3	18 ± 2	58.7 ± 9.5	0.31 ± 0.06
Yumen	T3	8.8 ± 1.2	13.0 ± 4.5	0.67 ± 0.2
	T5	21.4 ± 1.2	64.4 ± 9.0	0.33 ± 0.02
Bainan	T1	5.0	12.0 ± 2.0	0.41 ± 0.04
	T2	10.5	39.9 ± 5.8	0.27 ± 0.04
	T3	14.5	73.4 ± 8.8	0.20 ± 0.02
	T4	23.5	85.0 ± 9.8	0.28 ± 0.03
	T5	36	174.6 ± 18.2	0.21 ± 0.02

^aThe age of terrace T1 near the Bainan fault from Hetzel et al. (2002) and other offset and age data of terraces from our previous studies of Liu R. et al. (2017) and Chen and Koronovskii. (2020).

wide) and flat with a coarse gravel cover. We observed two to three terraces upstream and named them T1 to T3 from youngest to oldest (below naming terraces in the same way). Terraces T1 and T2 are widely distributed, but T3 can only be observed locally. The surfaces of terraces T1, T2, and T3 are 2–3, 7–10, and 20–30 m higher than the modern riverbed. The T1, T2, and T3 are accumulation terraces, which are mainly composed of fluvial gravel and covered with eolian loess (Figures 4D,G).

The middle reaches of the Baiyang river flow through the main mountain ranges of the northern Qilian Shan in which the valleys significantly narrow and the riverbeds that are more than 100 m wide upstream quickly narrow down to a width of 10 m in the midstream. Compared with the wide valleys upstream, deep and V-shaped valleys are developed in the midstream and the terrace type gradually changes from accumulation to erosion and basement terraces. Unconformities occur between the fluvial gravel and bedrock. The bedrock is composed of Paleozoic limestone, Mesozoic limestone and sandstone, Cenozoic orange sandstone, and Pleistocene conglomerate and the overlying layers consist of fluvial gravel and aeolian loess (Liu X.-w. et al., 2019). With the gradual increase in the terrace levels, high terraces are widely developed. In the south of the midstream, the number of terrace levels is 3–5. In the north of the midstream near the Hanxia fault, the terrace levels increase to 6–7. Terraces T1 to T7 are 2–3, 5–10, 20–30, 45–50, 65–75, 85–90, and up to 110 m above the modern riverbed, respectively (Figures 4C,F).

The lower reaches of the Baiyang river incise the piedmont alluvial fans of the northern Qilian Shan. In the range of the alluvial fans, the valleys widen and the types of valleys change from V-shaped valleys midstream to U-shaped valleys in the alluvial fan area. However, the gravel layer in the fan is relatively loose; thus, the valleys are still very deep. Low terraces downstream are poorly developed and only two high terraces are preserved. Based on the height of the river terraces, the two high terraces downstream can contrast with the T4 and T5 terraces in the midstream, 45–50 and 70–80 m above the modern riverbed, respectively. These terraces are mainly basement terraces. The basement is composed of Pleistocene conglomerates and the overlying layers consist of fluvial gravel and aeolian loess. After crossing the alluvial fan, the river flows

into the Jiuxi Basin and dries up in the middle of the basin (Figures 4B,E).

Based on the fluvial geomorphological characteristics of the Baiyang river, the fluvial geomorphic features in the middle reaches notably differ from those in the upper and lower reaches, mainly manifested by narrow, deep, and steep V-shaped valleys, an increase in the terrace level, wide distribution of high terraces, and different terrace types (mainly erosional and basement terraces). The above-mentioned characteristics indicate that the erosion in the middle reaches of the Baiyang river is more intense than that in the other reaches. As a regional river at the northern margin of the Qilian Shan, the Baiyang river has a similar regional climate and hydrodynamic environment, but the notable differences in the fluvial topography among the three reaches may be related to different intensities of tectonic movement, indicating that the northern Qilian Shan was subject to more intense tectonism.

4.3 Kinematics of Faults in the Baiyang River Catchment

From south to north, the Baiyang river flows through the Changma fault, northern Qilian fault (including the Hanxia fault and Yumen fault and associated Laojunmiao anticline), and Bainan fault and associated Baiyanghe anticline. The long-term slip rates of the faults since the Late Quaternary were determined (Liu R. et al., 2017; Chen and Koronovskii, 2020).

4.3.1 Changma Fault

The Changma fault with a total length of ~120 km is a sinistral strike-slip fault in the Qilian Shan with reverse components. Its western end is connected to the Altyn Tagh fault. The Changma fault is NWW-striking and inclined to the southwest, with a dip angle of 50°–70°. In the Baiyang river catchment, a fault plane can be observed along the Changma fault, with the occurrence of 165°±70° (Liu R. et al., 2017). Based on the fault plane, the Changma fault shows reverse faulting characteristics, that is, the Precambrian gray gneiss thrusts over the Miocene orange sandstone (Liu R. et al., 2017). Based on the longitudinal profile of the terraces near the Changma fault, we observed a significant vertical displacement of 18 ± 2 m for terrace T3 (Figure 5B). Combined with the age of T3 of 58.7 ± 9.5 ka obtained by the OSL dating method, the vertical slip rate of the Changma fault since ~59 ka was estimated to be 0.31 ± 0.06 mm/a and the horizontal shortening rate was determined to be 0.11 ± 0.02 mm/a (Table 1) (Liu R. et al., 2017). In addition, notable sinistral offset ridges and gullies can be observed on the eastern bank of the Baiyang river, indicating that the Changma fault is affected by sinistral strike-slip (Figure 5A). Based on the offsets and ages of the deformed terraces, the estimated sinistral strike-slip rate of the Changma fault is 3–5 mm/a in the Baiyang river catchment, which is in the eastern segment of the Changma fault (Figure 2) (Luo et al., 2013; Du et al., 2020).

4.3.2 Northern Qilian Fault

The northern Qilian fault is the boundary between the northern Qilian Shan and adjacent Jiuxi Basin, which controls the

geomorphologic contour of the study area. In the Baiyang river catchment, this fault can be divided into two NWW-striking secondary faults, that is, the Hanxia fault in the south and the Yumen thrust fault in the north (**Figure 6A**). Based on the fault scale, the Hanxia fault is the main boundary fault between the northern Qilian Shan and Jiuxi Basin. The Yumen fault is considered to be a newly formed thrust due to the northward expansion of the Qilian Shan (Chen and Koronovskii, 2020). Between the Hanxia and Yumen faults, the fault-related NWW-trending anticline fold (Laojunmiao anticline) is 7–10 km wide from south to north and ~50 km long from west to east (**Figure 6A**). The Hanxia fault, Yumen fault, and Laojunmiao anticline jointly constitute the northern Qilian frontal thrust system.

Based on topographic profiles, the river terraces along the Hanxia fault are insignificantly deformed, but distinct fault surfaces were observed in natural outcrops where the Ordovician limestone thrusts over the Yumen conglomerate of the Lower Pleistocene and the occurrence of the fault plane is $178^{\circ}\angle75^{\circ}$ (Liu R. et al., 2017). Based on geological mapping, the Hanxia fault has been inactive since the Pleistocene and active geomorphological evidence has not been found in the Baiyang valleys (Institute of Geology and Lanzhou Institute of Seismology, 1993). In addition, notable deformation cannot be observed for the terraces of the Shiyou river, a south–north river on the west side of the Baiyang river (Hetzell et al., 2006).

The activity of the Yumen fault and Laojunmiao anticline caused significant deformation the terraces of in the Baiyang river catchment. Although the Yumen fault is regarded as a blind thrust at the western front of the Qilian Shan (Liu X.-w. et al., 2019), we observed notable fault traces of the Yumen fault in the gullies on the east side of the Baiyang river, where the fault cuts through the gravel deposits of alluvial fans and its occurrence was measured to be $205^{\circ}\angle32^{\circ}$ (**Figure 6C**) (Chen and Koronovskii, 2020). Thrusting leads to the vertical displacement of the terraces of the Baiyang river. The longitudinal profile of the terraces of Baiyang river shows that T3, T4, and T5 along the Yumen fault were significantly deformed, with displacements of 8.8 ± 1.2 , 9.7 ± 1.1 , and 21.4 ± 1.2 m, respectively (**Figures 6B,D**). The abandonment ages of T3 and T5 obtained by terrestrial cosmogenic nuclide dating (^{10}Be) are 13.0 ± 4.5 and 64.4 ± 9.0 ka, respectively (**Table 1**) (Liu R. et al., 2017). Based on the dip angle of the fault, we determined the vertical slip and horizontal shortening rates of the Yumen fault since ~13 ka to be 0.67 ± 0.2 and 1.06 ± 0.5 mm/a, respectively. The vertical slip and horizontal shortening rates of the Yumen fault since ~64 ka were determined to be 0.33 ± 0.02 and 0.53 ± 0.03 mm/a, respectively (**Table 1**) (Chen and Koronovskii, 2020). Liu R. et al. (2017) constrained the vertical uplift and horizontal shortening rates of the Laojunmiao anticline since ~9 ka to be 1.23 ± 0.81 and 0.67 ± 0.02 mm/a, respectively. Based on the combination of the slip rates of the Hanxia fault, Yumen fault, and Laojunmiao anticline, the long-term vertical slip rate of the western part of the northern Qilian fault is 1.5–2 mm/a and the horizontal shortening rate is 1.2–1.7 mm/a, which is consistent with the shortening rate of 1.2–1.9 mm/a determined for the eastern segment of the Yumen fault (Liu X.-W. et al., 2017; Liu X.-w. et al., 2019; Liu X. et al.,

2019), slightly higher than the vertical slip rate of 0.9–1.3 mm/a and horizontal shortening rate of 1.1–1.4 mm/a reported for the middle segment of the northern Qilian fault since the Late Quaternary (Yang et al., 2018a) and significantly higher than the vertical uplift rate of 0.4–0.8 mm/a determined in the eastern part of the northern Qilian fault (Hu et al., 2015).

4.3.3 Bainan Fault

The Bainan fault is in the Jiuxi basin and has a NWW trend, northward dip, dip angle of 30° , and length of ~20 km (Liu R. et al., 2017). A fault-related fold (Baiyanghe anticline) is developed on the northern side of the Bainan fault (**Figure 7A**). The Bainan fault and Baiyanghe anticline, located on the alluvial fan in the center of the basin, considered to represent the reverse structure of the northern Qilian fault (Min et al., 2002). River erosion and tectonic movement may jointly result in the development and uplift of multiple terraces of the Baiyang river. However, its uplifting topographic expression contrasts sharply with the surrounding flat surface of the alluvial fan, indicating that the tectonic activity may play a crucial role in the growth of the fault and anticline. Therefore, we focus on the effects of the internal dynamics rather than the external dynamic process. From the longitudinal profiles, terraces T1–T5 are 5.0, 10.5, 14.5, 23.5, and 36 m above the modern riverbed (**Figures 7B,C**). The abandonment ages of T1–T5 based on terrestrial cosmogenic nuclide (^{10}Be) dating are 12.0 ± 2.0 , 39.9 ± 5.8 , 73.4 ± 8.8 , 85.0 ± 9.8 , and 174.6 ± 18.2 ka, respectively (**Table 1**) (Liu R. et al., 2017). Based on the combination of the heights and ages of the terraces, we determined the uplift rates of the Bainan fault and Baiyanghe anticline since the formation of T1–T5 to be 0.41 ± 0.04 , 0.27 ± 0.04 , 0.20 ± 0.02 , 0.28 ± 0.03 , and 0.21 ± 0.02 mm/a, respectively (**Table 1**) (Liu R. et al., 2017).

5 DISCUSSION

5.1 Deformation Characteristics of the Northwestern Qilian Shan

Based on the fluvial geomorphologic characteristics of the Baiyang river and the slip rates of faults, the vertical uplift rate of the northern Qilian Shan dominated by the northern Qilian fault is greater than that of the central Qilian Shan controlled by the Changma fault. On the one hand, the geomorphologic characteristics of the Baiyang river derived from the slope map and swath profiles of the western Qilian Shan based on DEM data suggest that the river erosion in the northern Qilian Shan is more intense than that in the central Qilian Shan and the terrain relief reaches a maximum in the northern Qilian Shan. On the other hand, the vertical slip rates of the Changma and the northern Qilian faults since the Late Pleistocene were estimated to be 0.31 ± 0.06 and $1.5\text{--}2$ mm/a, respectively, based on comparing the slip rates of the main faults in the Baiyang river catchment (Luo et al., 2013; Liu R. et al., 2017), demonstrating that the northern Qilian Shan has been uplifted faster than the central Qilian Shan.

Based on this study, the age of T3 along the Changma fault, that of T5 along the Yumen fault, and the average age of T2 and T3 along the Bainan fault are comparable (~60 ka). Based on the

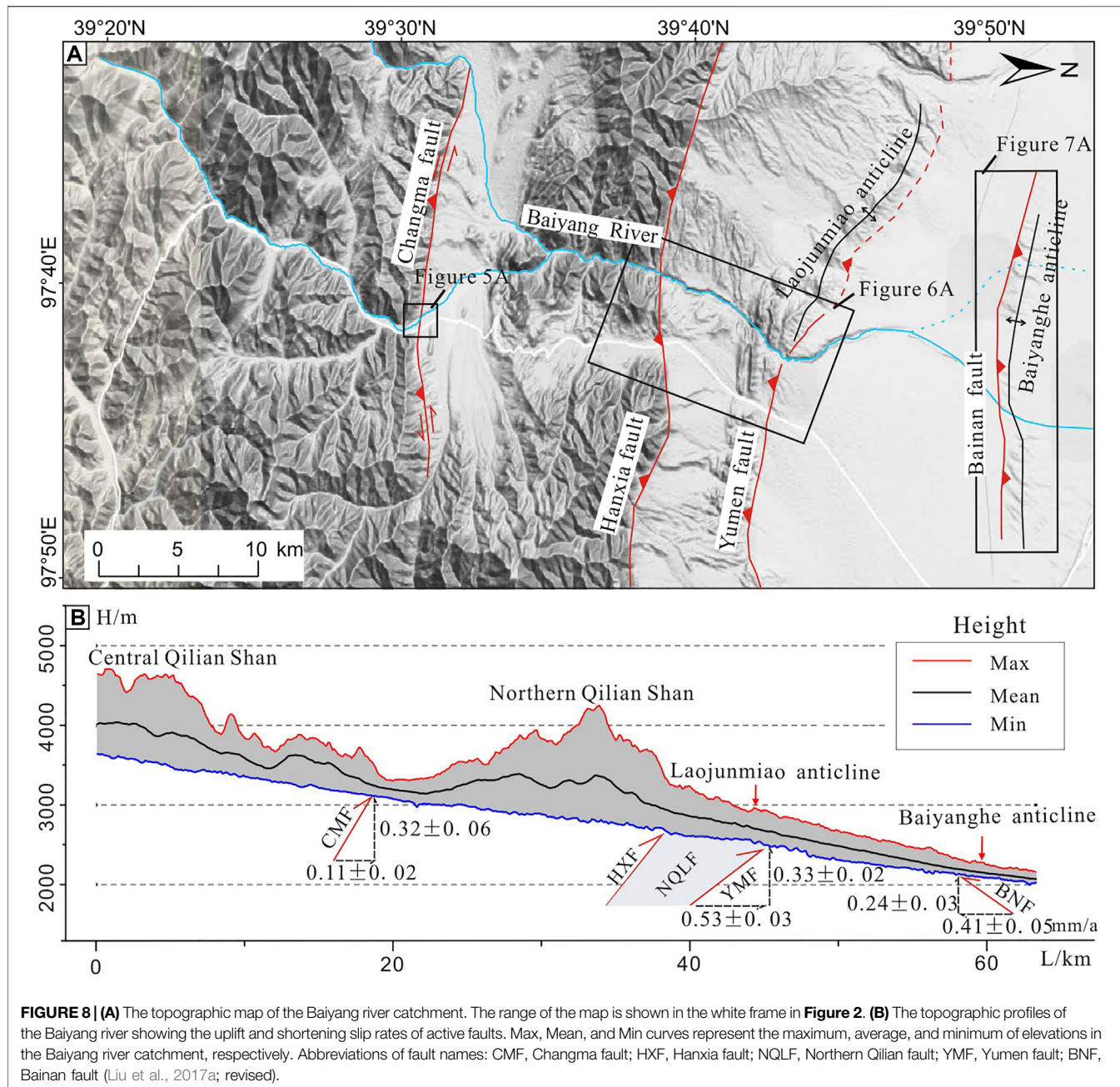
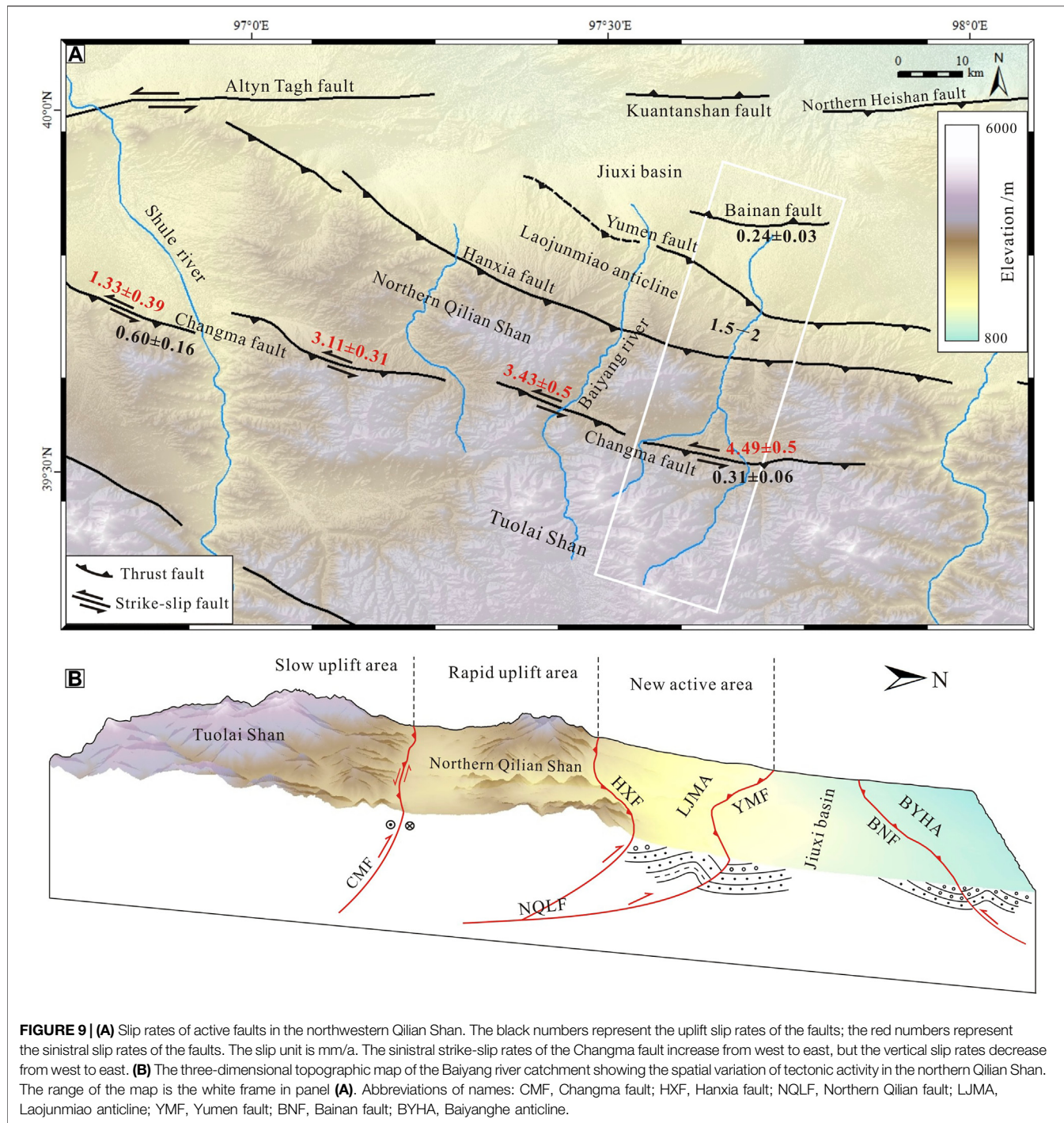


FIGURE 8 | (A) The topographic map of the Baiyang river catchment. The range of the map is shown in the white frame in **Figure 2**. **(B)** The topographic profiles of the Baiyang river showing the uplift and shortening slip rates of active faults. Max, Mean, and Min curves represent the maximum, average, and minimum of elevations in the Baiyang river catchment, respectively. Abbreviations of fault names: CMF, Changma fault; HXF, Hanxia fault; NQLF, Northern Qilian fault; YMF, Yumen fault; BNF, Bainan fault (Liu et al., 2017a; revised).

combination of the estimated fault slip rates with the dip angles, the vertical uplift rates of the Changma, Yumen, and Bainan faults since ~60 ka were estimated to be 0.31 ± 0.06 , 0.33 ± 0.02 , and 0.24 ± 0.03 mm/a, respectively, and the horizontal shortening rate were determined to be 0.11 ± 0.02 , 0.53 ± 0.03 , and 0.41 ± 0.05 mm/a, respectively (**Figures 8A,B**). Although the Hanxia fault might be the main fault based on its scale, a significant fault trace cannot be observed along the Hanxia fault (Hetzel et al., 2006; Liu R. et al., 2017; Liu X.-W. et al., 2017; Liu X.-W. et al., 2019). Instead, the Yumen fault and its anticline (Laojunmiao anticline) were notably deformed and their uplift and shortening rates since the Late Pleistocene are 1.5–2 and 1.2–1.7 mm/a,

respectively (**Figure 9A**) (Liu R. et al., 2017). Thus, both vertical uplift rates and shortening rates of the northern Qilian fault are significantly higher than those of the Changma fault within the Qilian Shan. However, it should be noted that the activity intensity of the Yumen fault at the northern Qilian Shan front is greater than that of the Hanxia fault (Hetzel et al., 2006). The reason for this phenomenon may be that the active area at the front of the northern Qilian Shan migrated from the Hanxia fault to the Yumen fault and associated fold belt due to the northward expansion of the Qilian Shan (**Figure 9B**).

Despite the relatively faster vertical uplift and horizontal shortening rates along the northern Qilian fault, a notable



strike-slip displacement has not been observed for this fault (Yang et al., 2018a). In contrast, the tectonic movement of the Changma fault resulted in notable sinistral displacements of ridges and gullies in the Baiyang river catchment. Based on the deformation and ages of the terraces along the Changma fault, the sinistral slip rates of the Changma fault in the western, middle, mid-eastern, and eastern segments were estimated to be 1.33 ± 0.39 , 3.11 ± 0.31 , 3.43 ± 0.5 , 4.49 ± 0.5 mm/a, respectively (Luo et al., 2013; Du et al., 2020). Conversely,

the vertical slip rate was estimated to be 0.60 ± 0.16 mm/a in the western segment and 0.31 ± 0.06 mm/a in the eastern segment (**Figure 9A**) (Luo et al., 2013; Liu R. et al., 2017). The sinistral strike-slip rates of the Changma fault gradually increase from west to east, whereas the vertical slip rates gradually decrease from west to east. Consequently, in the northwestern region of the Qilian Shan, crustal uplift and shortening largely occurred in the northern Qilian Shan and the range-bounding faults, but strike-slip occurred along the

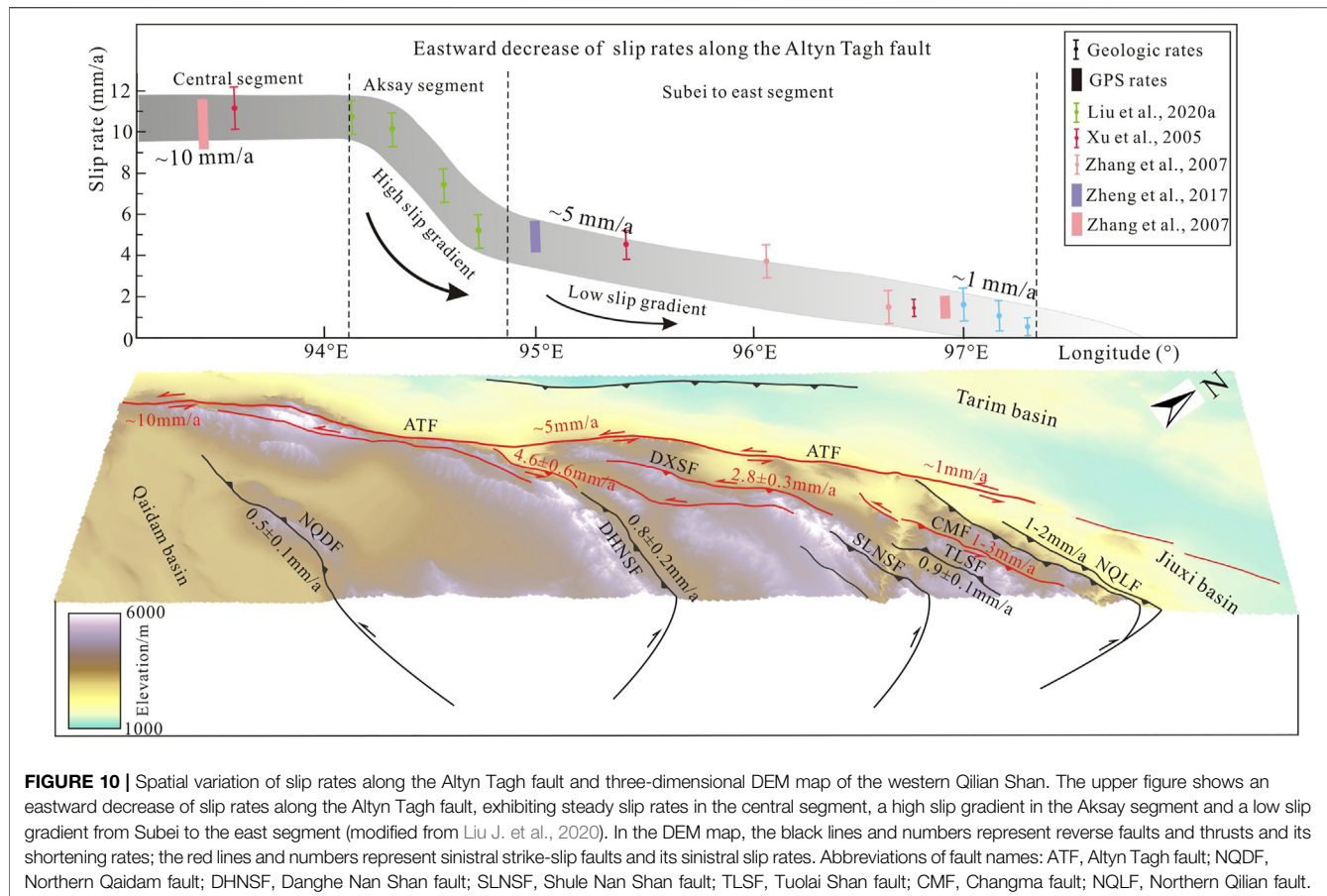


FIGURE 10 | Spatial variation of slip rates along the Altyn Tagh fault and three-dimensional DEM map of the western Qilian Shan. The upper figure shows an eastward decrease of slip rates along the Altyn Tagh fault, exhibiting steady slip rates in the central segment, a high slip gradient in the Aksay segment and a low slip gradient from Subei to the east segment (modified from Liu J. et al., 2020). In the DEM map, the black lines and numbers represent reverse faults and thrusts and its shortening rates; the red lines and numbers represent sinistral strike-slip faults and its sinistral slip rates. Abbreviations of fault names: ATF, Altyn Tagh fault; NQDF, Northern Qaidam fault; DHNSF, Danghe Nan Shan fault; SLNSF, Shule Nan Shan fault; TLSF, Tuolai Shan fault; CMF, Changma fault; NQLF, Northern Qilian fault.

Changma fault within the Qilian Shan, accommodating 1–3 mm/a of the sinistral strike-slip of the Altyn Tagh fault.

5.2 Deformation Pattern of the Western Qilian Shan in Response to the Crustal Shortening and Sinistral Strike-Slip of the Altyn Tagh Fault

The northern margin of the Tibetan Plateau consists of the Altyn Tagh fault, Qilian orogenic belts, and Haiyuan fault, which are characterized by large-scale lateral strike-slip, the uplift of NWW-trending mountains, and thrusting. However, the deformation pattern of the Qilian Shan in response to crustal shortening and sinistral strike-slip remains controversial because the strain partitioning in this region is poorly understood. The Qilian Shan is regarded to be a continental stepover between the Altyn Tagh and Haiyuan faults (Zhang et al., 2007). The GPS observations and geological investigations reveal that the Qilian Shan accommodates the sinistral slip rate component of ~8 mm/a of the Altyn Tagh fault and the strain is partitioned into the compressional deformation and sinistral strike-slip of the faults in the Qilian Shan (e.g., Zhang et al., 2007; Zheng et al., 2013b; Liu J. et al., 2020; Xu et al., 2021). Moreover, the GPS data also show NNE shortening at a rate of 5.5 ± 1.5 mm/a between the Qaidam Basin and Hexi Corridor, which is mainly absorbed by NWW-

trending mountain ranges and fault zones in the western Qilian Shan (Zhang et al., 2004).

The Altyn Tagh fault, as a large-scale boundary fault between the Tarim block to the north and the Tibetan Plateau to the south, plays an important role in controlling the tectonic deformation of the Tibetan Plateau during its northward growth. Two models, that is, the “eastward extrusion model” and “crust thickening model,” can be used to explain the deformation of the plateau. The “eastward extrusion model” is supported by the very high slip rates on the main boundary faults of the rigid blocks and the “crust thickening model” is characterized by continuous deformation distributed within the blocks as well as on the boundary faults, that is, a relatively low slip rate on the Altyn Tagh fault (Liu J. et al., 2020; Zhang et al., 2007). In recent years, results from geological studies, GPS observations, and interferometric synthetic aperture radar measurements suggested that the average slip rate of the Altyn Tagh is 8–10 mm/a on different timescales (e.g., Zhang et al., 2004; Xu et al., 2005; Zhang et al., 2007; Zheng et al., 2013b). This implies that the previous estimation of 20–30 mm/a may present an overestimation (e.g., Molnar et al., 1987; Peltzer and Tapponnier, 1989; Tapponnier et al., 2001). Most results show that the slip rate in the central part of the Altyn Tagh fault is relatively high and can reach 9–12 mm/a (Figure 10) (e.g., Zhang et al., 2007; Zheng et al., 2013b; Liu J. et al., 2020). Researchers

have noted an ununiform eastward decrease in the slip rate along the eastern segment of the Altyn Tagh fault, specifically at the junction of the Altyn Tagh fault and western Qilian Shan (e.g., Zhang et al., 2007; Zheng et al., 2013b; Liu J. et al., 2020). Liu et al. (2020a) revealed that the slip rate of the Altyn Tagh fault begins to significantly decrease in the Aksay segment in which the Altyn Tagh fault connects to the Danghe Nan Shan in the central Qilian Shan. In the Aksay–Subei segment, the slip rate of the Altyn Tagh fault decreases from 10 ± 1 to 5.1 ± 0.8 mm/a within a distance of 50 km. However, subsequently, the slip rate slowly decreases from ~5 mm/a in Subei to 1–2 mm/a in the easternmost segment of the Altyn Tagh fault (**Figure 10**) (Liu J. et al., 2020). Relatively low slip rates obtained along the Altyn Tagh fault suggest that the activity of the Altyn Tagh fault is not compatible with the “block extrusion model,” but supports the “crust thickening model.” In addition, the high decay of the slip rate in the eastern segment of the Altyn Tagh fault may be related to crustal thickening, thrusting, and left-lateral strike-slip in the Qilian Shan, resulting in blocking at this position (Liu J. et al., 2020).

The NNE-ward crustal shortening and sinistral strike-slip of the Altyn Tagh fault are mainly accommodated by NWW-trending mountains and fault zones in the western Qilian Shan. Understanding the strain partitioning of these faults is important for studying the deformation patterns in the northern plateau. From south to north, five large-scale NWW-trending fault zones are distributed in the western Qilian Shan, that is, the northern Qaidam, Danghenan Shan, Shulenhan Shan, Changma, and northern Qilian faults (**Figures 1B,C**). In most of the previous studies in the region, the focus was placed on boundary faults, especially the northern Qilian fault system, and the faulting or folding kinematics within the Qilian orogen were poorly documented. However, it is necessary to evaluate the deformation pattern in northeastern Tibet (Hu et al., 2021). The northern Qilian fault has a vertical slip rate of 0.8–1.4 mm/a and a shortening rate of 1–2 mm/a due to Late Quaternary geomorphic deformation (**Figure 10**) (e.g., Hetzel et al., 2002; Hetzel et al., 2004; Hetzel et al., 2006; Hu et al., 2015; Liu X.-W. et al., 2017; Yang et al., 2018a; Yang et al., 2018b; Hetzel et al., 2019; Liu X.-w. et al., 2019; Liu X. et al., 2019; Chen and Koronovskii, 2020; Liu R. et al., 2020; Yang et al., 2020; Hu et al., 2021), which is consistent with GPS data (e.g., Zheng et al., 2009; Pan et al., 2020) and the long-term shortening rate inferred from balanced cross-sections (Zuza et al., 2016). Notable horizontal strike-slip displacement has not been observed along the northern Qilian fault (Hetzel et al., 2006; Yang et al., 2018a). The results of previous studies showed that the northern Qilian fault has an eastward decreasing shortening rate, varying from 1.2–2 mm/a along the western segment to 0.8–1.4 mm/a in the central and eastern segments (e.g., Chen and Koronovskii, 2020; Hetzel et al., 2004; Hetzel et al., 2006; Hu et al., 2015; Liu R. et al., 2017; Liu X.-W. et al., 2017; Liu X. et al., 2019; Liu R. et al., 2020; Yang et al., 2018a; Yang et al., 2018b; Hetzel et al., 2019; Yang et al., 2020). The Changma fault, which is located in an intramontane basin within the western Qilian Shan, is characterized by left-lateral strike-slip with a thrust component. Its left-lateral strike-slip rates are 1.0–1.6 mm/a in the western segment and 3.0–4.9 mm/a in the eastern segment; however, the vertical slip rates vary from

0.6 ± 0.2 mm/a in the west to 0.3 ± 0.1 mm/a in the east (**Figure 9A**) (Luo et al., 2013; Du et al., 2020). Hu et al. (2021) derived a vertical slip rate of 1.5 ± 0.1 mm/a and a shortening rate of 0.9 ± 0.1 mm/a based on the deformation and ages of the terraces along the North Tuolai Shan fault (**Figure 10**), which is the boundary fault between the central and northern Qilian Shan mountains. This deformation rate is similar to the rates determined along the leading-edge fault in the northern Qilian Shan. To the west, a shortening rate of 2.1 ± 0.6 mm/a has been estimated for the northern frontal thrust system of the Daxue Shan (Meyer et al., 1998), which is aligned on the Tuolai Nan Shan and Shulenhan Shan, jointly constituting the boundary between the central Qilian Shan and southern Qilian Shan (Hu et al., 2021). By applying ^{10}Be exposure dating to samples from deformed river terraces, Xu et al. (2021) obtained a mean uplift rate of 0.6 ± 0.2 mm/a and a shortening rate of 0.8 ± 0.2 mm/a for the Danghe Nan Shan frontal thrust fault (**Figure 10**). The southern Zongwulong Shan thrust, the southern margin of the southern Qilian Shan, has a Holocene shortening rate of 0.5 ± 0.1 mm/a (Shao et al., 2019). Hu et al. (2021) suggested that the widely distributed shortening across the Qilian Shan supports the kinematics of distributed upper crustal shortening across the Qilian Shan, rather than a large, propagating crustal-scale deformation wedge.

In spite of the shortening rates of the main NWW-trending faults in the Qilian Shan varying in a similar range and the crustal shortening widely distributed across the Qilian Shan, the terrain relief shows that the crustal shortening varies in different orogenic belts within the Qilian Shan. The results of previous studies verified that crustal shortening, structural relief, and topographic relief correlate in mountain ranges, suggesting that crustal shortening is a primary driver of the uplift and topography of the Longmen Shan at the eastern margin of the Tibetan Plateau (Hubbard and Shaw, 2009). The slope map and swath profiles of the western Qilian Shan established in this study show that the terrain relief in the northern Qilian Shan is significantly higher than that in the central and southern orogenic belts. Specifically, the distribution of high-relief terrain and the relief values reach a maximum in the northern Qilian Shan, indicating that more intense mountain uplift and crustal shortening may occur in the northern Qilian Shan. Thus, we suggest that the crustal shortening in the northern Qilian Shan is more intense than that in the central and southern mountain ranges.

The northern Qilian Shan accounts for considerable crustal shortening in the northeastern Tibetan Plateau, whereas notable strike-slip has not been observed in the northern Qilian frontal region. Previous studies showed that the Qilian Shan accommodates the sinistral rate component of ~8 mm/a of the Altyn Tagh fault and transfers the strain into compressional deformation and sinistral strike-slip faults within the Qilian Shan (Liu J. et al., 2020; Zhang et al., 2007). It is necessary to determine the positions accommodating the eastward extrusion of the Altyn Tagh fault in the Qilian Shan. At the junctions between the Altyn Tagh fault and the western Qilian Shan, particularly the Danghe Nan Shan, Daxue Shan, and Changma faults, the slip rates of the Altyn Tagh fault significantly decrease (Hu et al., 2021; Zhang

et al., 2007). In contrast to the northern Qilian frontal thrust, notable sinistral strike-slip has been observed in these regions (Luo et al., 2013, 2015; Shao, 2010). Shao (2010) estimated the Holocene sinistral slip rate of the Danghe Nan Shan fault to be 4.55 ± 0.6 mm/a (**Figure 10**). Luo et al. (2013, 2015) determined the average left-lateral slip rate of the Daxue Shan fault and the slip rate of the Changma fault to be 2.81 ± 0.32 and 1–3 mm/a, respectively (**Figure 10**). These results show that the Danghe Nan Shan, Daxue Shan, and Changma faults within the Qilian Shan accommodate almost all sinistral slip rates of the Altyn Tagh fault (**Figure 10**). Liu J. et al. (2020) further suggested that the slip rate decrease along the Altyn Tagh fault is not uniform in junction segments. The slip rate decreases faster in the Aksay–Subei segment, at the intersection between the Altyn Tagh fault and Danghe Nan Shan, but it decreases slowly from Subei to the easternmost segment. Accordingly, the strike-slip of the three NWW-trending faults within the Qilian Shan, rather than the range-bounding faults, account for most of the strike-slip of the Altyn Tagh fault. However, the focus of previous studies was mainly placed on the northern boundary faults of the Qilian Shan and faulting or folding kinematics within the Qilian Shan were poorly documented, which limits our understanding of the tectonic deformation and strain partitioning in the Qilian Shan (Hu et al., 2021).

In summary, the compressional deformation of the Qilian Shan and strike-slip faults within the orogens is due to the NNE-ward crustal shortening of the northeastern Tibetan Plateau and the rapid sinistral strike-slip of the Altyn Tagh and Haiyuan faults. The crustal shortening across the Qilian Shan may be widely distributed in the NWW-trending compressional orogenic belts among which the northern Qilian Shan plays the most important role in absorbing crustal shortening because of its high-relief terrain and more rapid slip rate along the northern Qilian fault. Strike-slip faults within the Qilian Shan are key areas for the accommodation of the strike-slip of the Altyn Tagh fault through the sinistral strike-slip of faults and regional compressional deformation within the Qilian Shan. In addition, it is necessary to enhance the research of tectonic deformation within the Qilian Shan.

6 CONCLUSION

Spatial analysis and fluvial geomorphological studies are powerful tools for studying tectonic deformation within orogens. The topographic slope map and two swath profiles of the western Qilian Shan extracted from high-resolution DEM data show that the terrain relief in the northern Qilian Shan is significantly higher than that in the central and southern Qilian Shan. In addition, the fluvial geomorphologic characteristics of a north–south regional river (Baiyang river) illustrate that the stronger erosion in the middle reaches correlates with the rapid uplift of the northern Qilian Shan, demonstrating that the northern Qilian Shan has been uplifted more rapidly than the central Qilian Shan since the Late Quaternary. Based on high-resolution topographic measurements and chronological

constraints of deformed river terraces along faults in the western Qilian Shan, the vertical slip rates of the Changma, Yumen, and Bainan faults in the Baiyang river catchment since ~60 ka were estimated to be 0.31 ± 0.06 , 0.33 ± 0.02 , and 0.24 ± 0.02 mm/a, respectively. The comparison of our data with previously published results shows that the uplift rate of 1.5–2 mm/a of the northern Qilian fault is significantly higher than the uplift rate of 0.3–0.6 mm/a of the Changma fault within the Qilian Shan since the Late Quaternary, which matches the terrain relief in the Qilian Shan and demonstrates that the uplift rate of the northern Qilian Shan is higher than that of the central Qilian Shan. The slip rates of active faults in the western Qilian Shan reveal that the crustal shortening across the Qilian Shan may be widely distributed in the NWW-trending compressional orogenic belts and the northern Qilian Shan plays the most important role in absorbing crustal shortening; however, the rapid sinistral strike-slip of the Altyn Tagh fault is largely accommodated by strike-slip faults within the Qilian Shan.

DATA AVAILABILITY STATEMENT

The original contributions presented in the study are included in the article/Supplementary Material, further inquiries can be directed to the corresponding authors.

AUTHOR CONTRIBUTIONS

ZC is responsible for making the research plan, field work, sampling, writing the manuscript, and drawing the figures. WX is responsible for writing and revising the manuscript. RL is responsible for field work, sampling and dating, and drawing the figures. AL is responsible for the research plan, field work, and professional guidance. NK is responsible for professional guidance.

FUNDING

This research was financially supported by the National Key Research and Development Program of China (grant No. 2018YFC1504201), the National Natural Science Foundation of China (grant No. 41402185), the National Natural Science Foundation of China (grant No. 42174023), the National Key R&D Program of China (grant No. 2019YFC1509205), and China Scholarship Council (CSC).

ACKNOWLEDGMENTS

We are grateful to the editor, Wenjun Zheng, and three reviewers for providing valuable comments and suggestions on the manuscript. We thank Geospatial Data Cloud (<http://www.gscloud.cn/>) and USGS (<https://earthexplorer.usgs.gov/>) for providing the high-resolution DEM data and satellite images for this study.

REFERENCES

- Chen, Z., and Koronovskii, N. V. (2020). The Active Modern Faults of the Western Segment of the Qilian Mountains (North Tibet). *Mosc. Univ. Geol. Bull.* 75, 211–219. doi:10.3103/s0145875220030035
- Cheng, Q., Li, M., Li, F., and Tang, H. (2019). Response of Global Air Pollutant Emissions to Climate Change and its Potential Effects on Human Life Expectancy Loss. *Sustainability* 11 (13), 3670. doi:10.3390/su11133670
- Chu, Y. (2015). The Geomorphy Characteristic of Qilian Mountains and its Response to Tibetan Plateau Uplift (In Chinese). Doctor Dissertation thesis. Chengdu, Sichuan: Chengdu University of Technology.
- Ding, L., Maksatbek, S., Cai, F., Wang, H., Song, P., Ji, W., et al. (2017). Processes of Initial Collision and Suturing between India and Asia. *Sci. China Earth Sci.* 60 (4), 635–651. doi:10.1007/s11430-016-5244-x
- Du, J., Fu, B., Guo, Q., Shi, P., Xue, G., and Xu, H. (2020). Segmentation and Termination of the Surface Rupture Zone Produced by the 1932 Ms 7.6 Changma Earthquake: New Insights into the Slip Partitioning of the Eastern Altyn Tagh Fault System. *Lithosphere* 12 (1), 19–39. doi:10.1130/L1113.1
- England, P., and Houseman, G. (1986). Finite Strain Calculations of Continental Deformation: 2. Comparison with the India-Asia Collision Zone. *J. Geophys. Res.* 91 (B3), 3664–3676. doi:10.1029/JB091iB03p03664
- Harrison, T. M., Copeland, P., Kidd, W. S. F., and Yin, A. (1992). Raising Tibet. *Science* 255 (5052), 1663–1670. doi:10.1126/science.255.5052.1663
- Hetzl, R., Hampel, A., Gebbeken, P., Xu, Q., and Gold, R. D. (2019). A Constant Slip Rate for the Western Qilian Shan Frontal Thrust during the Last 200 Ka Consistent with GPS-Derived and Geological Shortening Rates. *Earth Planet. Sci. Lett.* 509, 100–113. doi:10.1016/j.epsl.2018.12.032
- Hetzl, R., Niedermann, S., Tao, M., Kubik, P. W., Ivy-Ochs, S., Gao, B., et al. (2002). Low Slip Rates and Long-Term Preservation of Geomorphic Features in Central Asia. *Nature* 417 (6887), 428–432. doi:10.1038/417428a
- Hetzl, R., Niedermann, S., Tao, M., Kubik, P. W., and Strecker, M. R. (2006). Climatic versus Tectonic Control on River Incision at the Margin of NE Tibet: ¹⁰Be Exposure Dating of River Terraces at the Mountain Front of the Qilian Shan. *J. Geophys. Res.* 111 (F3), F03012. doi:10.1029/2005jf000352
- Hetzl, R., Tao, M., Stokes, S., Niedermann, S., Ivy-Ochs, S., Gao, B., et al. (2004). Late Pleistocene/Holocene Slip Rate of the Zhangye Thrust (Qilian Shan, China) and Implications for the Active Growth of the Northeastern Tibetan Plateau. *Tectonics* 23 (6), TC6006. doi:10.1029/2004tc001653
- Hodges, K. V., Hurtado, J. M., and Whipple, K. X. (2001). Southward Extrusion of Tibetan Crust and its Effect on Himalayan Tectonics. *Tectonics* 20 (6), 799–809. doi:10.1029/2001TC001281
- Hu, X., Cao, X., Li, T., Mao, J., Zhang, J., He, X., et al. (2021). Late Quaternary Fault Slip Rate within the Qilian Orogen, Insight into the Deformation Kinematics for the NE Tibetan Plateau. *Tectonics* 40 (5), e2020TC006586. doi:10.1029/2020tc006586
- Hu, X., Pan, B., Kirby, E., Gao, H., Hu, Z., Cao, B., et al. (2015). Rates and Kinematics of Active Shortening along the Eastern Qilian Shan, China, Inferred from Deformed Fluvial Terraces. *Tectonics* 34 (12), 2478–2493. doi:10.1002/2015tc003978
- Hubbard, J., and Shaw, J. H. (2009). Uplift of the Longmen Shan and Tibetan Plateau, and the 2008 Wenchuan ($M = 7.9$) Earthquake. *Nature* 458 (7235), 194–197. doi:10.1038/nature07837
- Institute of Geology and Lanzhou Institute of Seismology (China Earthquake Administration) (1993). *Active Fault Systems in the Qilian Mountain-Hexi Corridor (In Chinese)*. Beijing: Seismological Press, 78.
- Lavé, J., and Avouac, J. P. (2001). Fluvial Incision and Tectonic Uplift across the Himalayas of Central Nepal. *J. Geophys. Res.* 106 (B11), 26561–26591. doi:10.1029/2001JB000359
- Li, A., Liu, R., and Zhang, S. (2021). Shortening Rate and Kinematics of the Active Huoshaogou Anticline, Northern Margin of the Tibetan Plateau, Inferred from Deformed Fluvial Terraces. *J. Asian Earth Sci.* 209, 104688. doi:10.1016/j.jseas.2021.104688
- Liu, J., Ren, Z., Zheng, W., Min, W., Li, Z., and Zheng, G. (2020). Late Quaternary Slip Rate of the Aksay Segment and its Rapidly Decreasing Gradient along the Altyn Tagh Fault. *Geosphere* 16 (6), 1538–1557. doi:10.1130/ges02250.1
- Liu, R., Li, A., Zhang, S., Chen, Z., and Guo, C. (2017). The Late Quaternary Tectonic Deformation Revealed by the Terraces on the Baiyang River in the Northern Qilian Mountains. *Seismol. Geol.* 39 (6), 1237–1255. doi:10.3969/j.issn.0253-4967.2017.06.010
- Liu, R., Li, A., Zhang, S., Guo, C., and Chen, Z. (2020). A NW-Striking Dextral Strike-Slip Fault at the Eastern End of the Altyn Tagh Fault and its Tectonic Implications for Northeastward Growth of the Tibetan Plateau. *J. Asian Earth Sci.* 188, 104069. doi:10.1016/j.jseas.2019.104069
- Liu, X.-W., Yuan, D.-Y., and Su, Q. (2017). Late Pleistocene Slip Rate of the Northern Qilian Shan Frontal Thrust, Western Hexi Corridor, China. *Terra Nova* 29 (6), 238–244. doi:10.1111/ter.12270
- Liu, X.-W., Yuan, D.-Y., and Su, Q. (2019). Late Pleistocene Slip Rate on a Blind Thrust in the Western Qilian Shan, NW China. *Geomorphology* 345, 106841. doi:10.1016/j.geomorph.2019.106841
- Liu, X., Yuan, D., Zheng, W., Shao, Y., Liu, B., and Gao, X. (2019). Holocene Slip Rate of the Frontal Thrust in the Western Qilian Shan, NE Tibetan Plateau. *J. Asian Earth Sci.* 219, 853–865. doi:10.1093/gji/ggz325
- Luo, H., He, W., Wang, D., Yuan, D., and Shao, Y. (2013). Study on the Slip of Changma Fault in Qilian Mountains since Late Pleistocene. *Seismol. Geol.* 35 (4), 765–777. doi:10.3969/j.issn.0253-4967.2013.04.007
- Luo, H., He, W., Yuan, D., and Shao, Y. (2015). Slip Rate of Yema River-Daxue Mountain Fault since the Late Pleistocene and its Implications on the Deformation of the Northeastern Margin of the Tibetan Plateau. *Acta Geologica Sinica - English Edition* 89 (2), 561–574. doi:10.1111/1755-6724.12447
- Meyer, B., Tapponnier, P., Bourjot, L., Métivier, F., Gaudemer, Y., Peltzer, G., et al. (1998). Crustal Thickening in Gansu-Qinghai, Lithospheric Mantle Subduction, and Oblique, Strike-Slip Controlled Growth of the Tibet Plateau. *Geophys. J. Int.* 135, 1–47. doi:10.1046/j.1365-246X.1998.00567.x
- Min, W., Zhang, P., He, W., Li, C., Mao, F., and Zhang, S. (2002). Research on the Active Faults and Paleoearthquakes in the Western Jiuquan Basin. *Seismol. Geol.* 24 (1), 35–44. doi:10.3969/j.issn.0253-4967.2002.01.004
- Molnar, P., Burchfiel, B. C., Kuangyi, L., and Ziyun, Z. (1987). Geomorphic Evidence for Active Faulting in the Altyn Tagh and Northern Tibet and Qualitative Estimates of its Contribution to the Convergence of India and Eurasia. *Geol* 15 (3), 249–253. doi:10.1130/0091-7613(1987)15<249:gefati>2.0.co;2
- Molnar, P., and Tapponnier, P. (1975). Cenozoic Tectonics of Asia: Effects of a Continental Collision: Features of Recent continental Tectonics in Asia Can Be Interpreted as Results of the India-Eurasia Collision. *Science* 189, 419–426. doi:10.1126/science.189.4201.419
- Pan, Z., Yun, Z., and Shao, Z. (2020). Contemporary Crustal Deformation of Northeast Tibet from Geodetic Investigations and a Comparison between the Seismic and Geodetic Moment Release Rates. *Phys. Earth Planet. Interiors* 304, 106489. doi:10.1016/j.pepi.2020.106489
- Peltzer, G., Tapponnier, P., and Armijo, R. (1989). Magnitude of Late Quaternary Left-Lateral Displacements along the North Edge of Tibet. *Science* 246 (4936), 1285–1289. doi:10.1126/science.246.4935.1285
- Shao, Y., Li, Z., Zhang, B., Wang, P., Yuan, D., and Wu, M. (2019). Paleoseismological Study of the Southern Zongwulong Shan Fault, Qilian Mountains, Western China. *Geomorphology* 326, 107–115. doi:10.1016/j.geomorph.2017.12.036
- Shao, Y. (2010). The Activity Features during Late Quaternary of Yema River-Danghe Nan Shan Faults in Western Qilian Shan (In Chinese). Master Dissertation thesis. Lanzhou, Gansu: Lanzhou Institute of Seismology.
- Tapponnier, P., and Molnar, P. (1976). Slip-line Field Theory and Large-Scale Continental Tectonics. *Nature* 264, 319–324. doi:10.1038/264319a0
- Tapponnier, P., Zhiqin, X., Roger, F., Meyer, B., Arnaud, N., Wittlinger, G., et al. (2001). Oblique Stepwise Rise and Growth of the Tibet Plateau. *Science* 294 (5547), 1671–1677. doi:10.1126/science.105978
- Wang, C., Dai, J., Zhao, X., Li, Y., Graham, S. A., He, D., et al. (2014). Outward-growth of the Tibetan Plateau during the Cenozoic: A Review. *Tectonophysics* 621 (complete), 1–43. doi:10.1016/j.tecto.2014.01.036
- Wang, M., and Shen, Z. K. (2020). Present-Day Crustal Deformation of Continental China Derived from GPS and its Tectonic Implications. *J. Geophys. Res. Solid Earth* 125 (2), e2019JB018774. doi:10.1029/2019jb018774
- Wang, W., Zhang, P., Pang, J., Garzzone, C., Zhang, H., Liu, C., et al. (2016). The Cenozoic Growth of the Qilian Shan in the Northeastern Tibetan Plateau: A

- Sedimentary Archive from the Jiuxi Basin. *J. Geophys. Res. Solid Earth* 121 (4), 2235–2257. doi:10.1002/2015JB012689
- Xu, Q., Hetzel, R., Hampel, A., and Wolff, R. (2021). Slip Rate of the Danghe Nan Shan Thrust Fault from 10 Be Exposure Dating of Folded River Terraces: Implications for the Strain Distribution in Northern Tibet. *Tectonics* 40 (4), e2020TC006584. doi:10.1029/2020tc006584
- Xu, X., Wang, F., Zheng, R., Chen, W., Ma, W., Yu, G., et al. (2005). Late Quaternary Sinistral Slip Rate along the Altyn Tagh Fault and its Structural Transformation Model. *Sci. China Ser. D-earth Sci.* 48 (3), 384–397. doi:10.1360/02yd0436
- Yang, H., Yang, X., Huang, W., Li, A., Hu, Z., Huang, X., et al. (2020). 10Be and OSL Dating of Pleistocene Fluvial Terraces along the Hongshuiba River: Constraints on Tectonic and Climatic Drivers for Fluvial Downcutting across the NE Tibetan Plateau Margin, China. *Geomorphology* 348, 106884. doi:10.1016/j.geomorph.2019.106884
- Yang, H., Yang, X., Huang, X., Li, A., Huang, W., and Zhang, L. (2018a). New Constraints on Slip Rates of the Fodongmiao-Hongyazi Fault in the Northern Qilian Shan, NE Tibet, from the 10Be Exposure Dating of Offset Terraces. *J. Asian Earth Sci.* 151, 131–147. doi:10.1016/j.jseas.2017.10.034
- Yang, H., Yang, X., Zhang, H., Huang, X., Huang, W., and Zhang, N. (2018b). Active Fold Deformation and Crustal Shortening Rates of the Qilian Shan Foreland Thrust Belt, NE Tibet, since the Late Pleistocene. *Tectonophysics* 742–743, 84–100. doi:10.1016/j.tecto.2018.05.019
- Yin, A., and Harrison, T. M. (2000). Geologic Evolution of the Himalayan-Tibetan Orogen. *Annu. Rev. Earth Planet. Sci.* 28, 211–280. doi:10.1146/annurev.earth.28.1.211
- Zhang, P.-Z., Molnar, P., and Xu, X. (2007). Late Quaternary and Present-Day Rates of Slip along the Altyn Tagh Fault, Northern Margin of the Tibetan Plateau. *Tectonics* 26 (5), TC5010. doi:10.1029/2006tc002014
- Zhang, P.-Z., Shen, Z., Wang, M., Gan, W., Bürgmann, R., Molnar, P., et al. (2004). Continuous Deformation of the Tibetan Plateau from Global Positioning System Data. *Geol* 32 (9), 809–812. doi:10.1130/g20554.1
- Zheng, D., Wang, W., Wan, J., Yuan, D., Liu, C., Zheng, W., et al. (2017). Progressive Northward Growth of the Northern Qilian Shan-Hexi Corridor (Northeastern Tibet) during the Cenozoic. *Lithosphere* 9 (3), 408–416. doi:10.1130/1587.1
- Zheng, W., Zhang, H., Zhang, P., Molnar, P., Liu, X., and Yuan, D. (2013a). Late Quaternary Slip Rates of the Thrust Faults in Western Hexi Corridor (Northern Qilian Shan, China) and Their Implications for Northeastward Growth of the Tibetan Plateau. *Geosphere* 9 (2), 342–354. doi:10.1130/ges00775.1
- Zheng, W., Zhang, P., He, W., Yuan, D., Shao, Y., Zheng, D., et al. (2013b). Transformation of Displacement between Strike-Slip and Crustal Shortening in the Northern Margin of the Tibetan Plateau: Evidence from Decadal GPS Measurements and Late Quaternary Slip Rates on Faults. *Tectonophysics* 584, 267–280. doi:10.1016/j.tecto.2012.01.006
- Zheng, W., Zhang, P., Yuan, D., and Zheng, D. (2009). Deformation on the Northern of the Tibetan Plateau from GPS Measurement and Geologic Rates of Late Quaternary along the Major Fault. *Chin. J. Geophys.* 52 (10), 2491–2508. doi:10.3969/j.issn.0001-5733.2009.10.008
- Zuza, A. V., Cheng, X., and Yin, A. (2016). Testing Models of Tibetan Plateau Formation with Cenozoic Shortening Estimates across the Qilian Shan-Nan Shan Thrust belt. *Geosphere* 12 (2), 501–532. doi:10.1130/ges01254.1

Conflict of Interest: Author RL was employed by Northwest Electric Power Design Institute Co. Ltd.

The remaining authors declare that the research was conducted in the absence of any commercial or financial relationships that could be construed as a potential conflict of interest.

Publisher's Note: All claims expressed in this article are solely those of the authors and do not necessarily represent those of their affiliated organizations, or those of the publisher, the editors, and the reviewers. Any product that may be evaluated in this article, or claim that may be made by its manufacturer, is not guaranteed or endorsed by the publisher.

Copyright © 2022 Chen, Xu, Liu, Li and Koronovsky. This is an open-access article distributed under the terms of the Creative Commons Attribution License (CC BY). The use, distribution or reproduction in other forums is permitted, provided the original author(s) and the copyright owner(s) are credited and that the original publication in this journal is cited, in accordance with accepted academic practice. No use, distribution or reproduction is permitted which does not comply with these terms.